

INFRARED PHOTOMETRY OF β PICTORIS TYPE SYSTEMS

S. B. FAJARDO-ACOSTA¹

Department of Physics and Astronomy, University of Denver, 2112 East Wesley Avenue, Denver, CO 80208; and Behrend School of Science, Pennsylvania State University Erie, Station Road, Erie, PA 16563; sergio@quesito.phys.du.edu

C. M. TELESCO¹

Department of Astronomy, University of Florida, 211 Space Sciences Building, Gainesville, FL 32611; telesco@astro.ufl.edu

AND

R. F. KNACKE¹

Behrend School of Science, Pennsylvania State University Erie, Station Road, Erie, PA 16563; rfk2@psu.edu

Received 1997 August 29; revised 1998 February 3

ABSTRACT

We obtained small-aperture (4"–5" diameter) infrared (2–20 μm) photometry of 10 early-type main-sequence stars with infrared excesses from circumstellar dust. These systems possibly exemplify the β Pictoris phenomenon. We observed them with either the NASA Marshall Space Flight Center bolometer array camera ("Big Mac") or the Infrared Telescope Facility 2–30 μm single-channel bolometer system. Measurements were obtained in the *KLMNQ* filters and the narrowband ($\Delta\lambda \approx 1 \mu\text{m}$) 10 μm "silicate" filters. We fitted Kurucz photospheric models to the photometric data to determine excess-emission spectra. We report the nondetection of small-aperture circumstellar dust emission from HR 10 and 21 LMi. We confirmed previous nondetections of near-infrared or 10 μm excess emission from 68 Oph, α PsA, and HR 4796A. We did not detect prominent silicate emission from any of the sources. The spectra of γ Oph, σ Her, HR 2174A, β UMa, and ζ Lep show weak 10 μm excesses. We fitted simple models to these data, together with *IRAS* excess fluxes, to determine plausible distributions of temperature and density of circumstellar dust grains. Significant quantities of these grains around HR 2174A, ζ Lep, and β UMa are at temperatures similar to terrestrial material in the solar system.

Key words: circumstellar matter — dust, extinction — infrared radiation — stars: early-type

1. INTRODUCTION

There are more than 100 main-sequence stars of all spectral types with *IRAS* excesses (Aumann et al. 1984; Aumann 1985; Gillett 1986; Backman & Gillett 1987; Walker & Wolstencroft 1988; Backman & Paresce 1993). Among them, β Pictoris (A5 V) and other systems show excess emission in the *IRAS* 12 μm bandpass. These excesses are thus accessible for ground-based follow-up through the atmospheric 10 μm "window." This spectral region includes features of solids such as the 8–13 μm silicate feature and the 7.7, 8.6, and 11.2 μm polycyclic aromatic hydrocarbon (PAH) features. Spectroscopy of solids in β Pic and similar systems offers a means to study directly the mineralogy, particle sizes, and spatial distribution of dust grains around the stars. The mineralogy in these systems can be compared with that of dust around evolved stars, pristine interstellar dust, and solar system dust. Determination of the composition and structure of Vega-like dust disks has wide-ranging implications for the evolution of disks in young stellar objects, star and planet formation, and the origins of the solar system.

Observations of dust at 10 μm let us probe material around other stars at temperatures similar to terrestrial material in our solar system. These observations will be relevant to the eventual search for Earth-like extrasolar planets, and how this dust will interfere in such searches (Backman 1998).

Telesco & Knacke (1991, hereafter TK) obtained narrow-

band ($\Delta\lambda \approx 1 \mu\text{m}$) photometry of β Pic in several of the "silicate" filters spanning the 8–13 μm region. They discovered a 10 μm silicate emission feature from β Pic. Within the limitations of narrowband photometry, the circumstellar silicate feature of β Pic strongly resembled the feature observed in comet Halley (Campins & Ryan 1989) and possibly in Kohoutek (Merrill 1974). Knacke et al. (1993) and Aitken et al. (1993) subsequently obtained 10 μm intermediate-resolution ($R = \lambda/\Delta\lambda \approx 50$) spectroscopy of β Pic, confirming the similarity of the silicate feature to those in comets Halley, Bradfield 1987s, and Levy 1990 XX (see Hanner, Lynch, & Russell 1994 for a review on cometary silicate spectroscopy). The 10 μm silicate feature of β Pic and the aforementioned comets extends from ~ 8 to 12.5 μm and shows a main peak at $\sim 9.5 \mu\text{m}$ and a secondary peak at 11.3 μm . The 11.3 μm peak in these sources is attributed to crystalline olivine (e.g., Campins & Ryan 1989; Knacke et al. 1993; Hanner et al. 1994).

Fajardo-Acosta, Telesco, & Knacke (1993, hereafter FTK) obtained 2–20 μm narrowband photometry of 51 Oph (B9.5 V). The photometry of 51 Oph showed a prominent 10 μm silicate emission feature, possibly resembling that in β Pic (TK). Subsequent 10 μm ground-based spectra ($R \approx 50$) of 51 Oph (Walker & Butner 1995; Sylvester et al. 1996; Fajardo-Acosta 1996; Russell et al. 1998) showed a silicate emission feature as broad as β Pic's with a main peak near 9.5 μm . The 51 Oph spectrum measured by Fajardo-Acosta and Russell et al. also showed an 11.3 μm peak, attributed to crystalline olivine. The presence of this peak and the above interpretation were confirmed by spectroscopy at $R \approx 200$ with the *Infrared Space Observatory (ISO)* Short Wavelength Spectrograph, by Waelkens et al. (1996).

¹ Visiting Astronomer at the Infrared Telescope Facility, which is operated by the University of Hawaii under contract to the National Aeronautics and Space Administration.

It is not yet known how commonly other main-sequence stars emit β Pic-like $10\ \mu\text{m}$ silicate features. Ten-micron spectra of systems such as HD 98800, K5 V (Skinner, Barlow, & Justanont 1992; Zuckerman & Becklin 1993), and SAO 26804 (K2 V; Skinner et al. 1995) show weak silicate features that are difficult to characterize. The $10\ \mu\text{m}$ silicate feature of the A9/F0 V star SAO 184124 (Sylvester et al. 1996) does not resemble that in β Pic. It shows only the $9.5\ \mu\text{m}$ peak and is more similar to the interstellar silicate emission feature modeled by Draine & Lee (1984). The $10\ \mu\text{m}$ spectra of other main-sequence stars show 7.7, 8.7, and $11.3\ \mu\text{m}$ emission features attributable to carbonaceous material. Examples of such systems are the B9 V star SAO 186777 (Sylvester et al. 1996), the F8 V stars SAO 26804 (Skinner et al. 1995) and SAO 206462 (Coulson & Walther 1995), and the B9 V star HD 100546 (Waelkens et al. 1996). The $11.3\ \mu\text{m}$ feature of the latter is also partially attributable to crystalline olivine (Waelkens et al. 1996).

In order to draw general conclusions about the $10\ \mu\text{m}$ emission in main-sequence stars, high signal-to-noise ratio (S/N) spectra of more systems are needed for further comparisons. To support such observations, we conducted a $10\ \mu\text{m}$ narrowband ($\Delta\lambda \approx 1\ \mu\text{m}$) photometric survey of the excess emission of main-sequence stars. Our survey complements broadband ($\Delta\lambda \sim 10\ \mu\text{m}$) photometric searches with *ISO* for excesses from main-sequence stars, such as the 25–180 μm observations by Habing et al. (1996) of α Lyr (A0 V) and g Lup (F5 IV–V), among other sources. The results of our survey will aid in the preparation and interpretation of higher resolution ground- and space-based follow-up $10\ \mu\text{m}$ spectroscopy work. The 8–12 μm spectroscopic observations ($R \sim 200$ –1000) of 51 Oph and HD 100546 with *ISO* (Waelkens et al. 1996) exemplify the kind of data for sources with bright $10\ \mu\text{m}$ excesses, greater than ~ 10 Jy, that are becoming available. For the present survey we selected systems presumably similar to β Pic. The stars are of early spectral type (B and A), they have modest $12\ \mu\text{m}$ *IRAS* excesses (< 1 Jy), and in some cases they show episodic UV and optical redshifted absorption lines suggesting plasma infall onto the star, as in the case of β Pic (Lagrange-Henri, Vidal-Madjar, & Ferlet 1988, among others). It has not always been determined whether the observed *IRAS* excesses from these systems are due to circumstellar material or to background sources contaminating the large *IRAS* beam. The *IRAS* Faint Source Survey and the ADDSCAN/SCANPI software have, in some instances, strengthened the possibility that the infrared excesses of some of these stars are from circumstellar material. Only in a few cases is $10\ \mu\text{m}$ photometry available to corroborate putative detections of circumstellar dust by *IRAS*.

Our ground-based small-aperture mid- and near-infrared photometry survey presented here serves three purposes: first, it can confirm that *IRAS* excesses originate from within the immediate vicinity of the stars; second, it allows us to quantify the amount of circumstellar material emitting in the infrared; and third, observations in the narrowband $10\ \mu\text{m}$ silicate filters, and subsequent intermediate-resolution spectroscopy, can lead to the identification of silicate emission (or other prominent emission features, such as those from PAHs).

2. OBSERVATIONS

In Table 1, we summarize our selection of sources and previous observational evidence that merited their inclusion

in our observing list. The excess flux densities of our targets near $10\ \mu\text{m}$ (where the silicate feature was searched for) were initially estimated from their *IRAS* $12\ \mu\text{m}$ fluxes and the $V - [12]$ relations for normal O, B, and A stars (Waters, Coté, & Aumann 1987). Visual magnitudes were corrected for interstellar reddening (as explained in § 3.1) before applying the above relations. In some cases ground-based K and N photometry was available to corroborate or refine the excesses (see references to Table 1). The assumption here was that $K - N = 0$ (within ~ 0.06 mag, based on photometric statistical uncertainties) for A0–G2 main-sequence stars (Johnson 1966; Aumann & Probst 1991). Atmospheric models for α Lyr (A0 V) and α CMa (A1 V), of comparable spectral type to our late B- and A-type sources, predict that $K - N = 0$ within 0.01 mag (Cohen et al. 1992).

Observations were conducted at the NASA Infrared Telescope Facility (IRTF) in 1992 September, 1993 March–April, and 1993 July. For the September set, we used the mid-infrared bolometer array camera (“Big Mac”), developed at NASA Marshall Space Flight Center. For the 1993 observations, we used the 2–30 μm IRTF bolometer system. We observed a total of 10 Vega-type stars during the three runs. In Table 2, we summarize the list of targets, their observation dates, and the instrument utilized.

The Big Mac camera consists of an array of 20 germanium bolometers (5×4 in R.A. \times decl.), each pixel subtending 3.9×4.2 (R.A. \times decl.). Targets were placed in a particularly sensitive pixel of the array, and the other 19 pixels were used to monitor and subtract certain components of sky and telescope noise that were correlated among the pixels (TK). No attempt was made to spatially resolve the sources with the array. The chopping frequency during Big Mac observations was 10 Hz, and the chopper throw was $15''$. The measured beam diameter during the IRTF bolometer observations was $5''$ (FWHM). The IRTF bolometer data were taken with a chopping frequency of 13 Hz and a chopper throw of $10''$.

Photometric data were obtained in the intermediate-bandpass “silicate” filters spanning the 8–13 μm region and broadband 10 and 20 μm filters listed in Table 3. In addition, we obtained near-infrared photometry at K ($2.2\ \mu\text{m}$), L ($3.45\ \mu\text{m}$), and M ($4.80\ \mu\text{m}$) during observations with the IRTF bolometer. Photometric standards were chosen from the IRTF Photometry Manual (Tokunaga 1986) based on their proximity to the targets. For the absolute flux calibration we assumed that the flux density values of α Lyr in the IRTF Photometry Manual correspond to zero magnitude in the mid-infrared bandpasses. The magnitudes of other standards in the above reference are available only in the broadband N and Q filters (Table 3, bottom). If α Lyr was measured sufficiently close in time and/or air mass to other standards, then these were calibrated against the former in all filters. To interpolate zero-magnitude fluxes from the IRTF bolometer bandpasses to the Big Mac bandpasses in Table 3, we assumed a 10^4 K blackbody energy distribution.

Extinction coefficients for Big Mac photometry were obtained from UT 1992 September 9 observations of α Lyr, whose air mass ranged from 1.3 to 1.9. These coefficients were then applied to the data of all three nights in 1992 September. We did not measure extinction coefficients at $10.3\ \mu\text{m}$. For IRTF bolometer photometry, we obtained nightly extinction coefficients from observations of α Lyr and/or μ UMa. On UT 1993 April 6 we did not obtain

TABLE 1
 β PICTORIS ANALOGS

Name	Spectral Type	V Magnitude	D (pc)	Reference	Comments
σ Her	B9 V	4.20	100	1	<i>IRAS</i> Point Source Catalog (PSC) fluxes from circumstellar (CS) dust. UV absorptions from infalling plasma
γ Oph	A0 V	3.75	26 ± 6	2	<i>IRAS</i> excess flux. Weak Ca II and Na I absorptions of unknown origin (either CS or interstellar [IS])
HR 4796A	A0 V	5.81	76	3	Large IR fluxes in the <i>IRAS</i> PSC and Serendipitous Survey Catalog; CS dust τ twice that of β Pic (Jura 1991). CS 20 μ m excess confined within 5" from the star (Jura et al. 1993). Dust grains larger than IS ones; possible hole 40 AU in radius in the CS dust region (Jura et al. 1995)
β UMa	A1 V	2.37	19 ± 8	4	<i>IRAS</i> excess at 60 μ m. Nearly zero 12 μ m excess, but large total flux
ζ Lep	A2 Vann	3.55	24 ± 8	5	<i>IRAS</i> 12 μ m excess confirmed with ground-based 10 μ m photometry
68 Oph	A2 Vn	4.45	48 ± 19	6	Putative visual detection of edge-on disk (Vidal-Madjar et al. 1993); not confirmed in subsequent observation (Vidal-Madjar et al. 1995). No excess in <i>IRAS</i> PSC (Vidal-Madjar et al. 1993) or <i>IRAS</i> GYPSY fluxes (Waters et al. 1995)
HR 10	A2 IV/V	6.19	70	7	Shell star. Optical Ca II and Na I line absorptions of infalling plasma. IR excess detected from <i>IRAS</i> Faint Source Survey
α PsA	A3 V	1.15	7.0 ± 0.3	8	<i>IRAS</i> excess at 60 μ m; small 12 μ m excess, but large total flux
HR 2174A	A3 V	5.73	72	2	Optical Ca II and Na I line absorptions analogous to β Pic's. <i>IRAS</i> PSC fluxes show confusion with field sources
21 LMi	A7 V	4.48	26 ± 3	5	<i>IRAS</i> excess at 12 μ m. Need to confirm excess with small-aperture photometry

NOTES.—Spectral type, V magnitude, and distance from Hoffleit & Jaschek 1982 and/or the SIMBAD database, except as noted below. Uncertainties of trigonometric parallax distance measurements are from Jenkins 1963. Distances quoted without uncertainty are spectroscopic parallax measurements from the listed references. The last column describes observational evidence of possible β Pic-like characteristics.

REFERENCES.—(1) Grady et al. 1991; (2) Lagrange-Henri et al. 1990; (3) Jura 1991; (4) Aumann & Probst 1991; (5) Aumann & Probst 1991; (6) Vidal-Madjar et al. 1993; (7) Cheng et al. 1991; (8) Gillett 1986.

TABLE 2
LOG OF IRTF OBSERVATIONS

HR	Name	UT Dates of Observation	Instrument ^a
1998.....	ζ Lep	1992 Sep 7, 8, 9	Big Mac
		1993 Apr 4	IRTF bolo
10.....		1992 Sep 8	Big Mac
8728.....	α PsA	1992 Sep 7, 8	Big Mac
6168.....	σ Her	1993 Apr 1, 4	IRTF bolo
3974.....	21 LMi	1993 Apr 1	IRTF bolo
6629.....	γ Oph	1993 Apr 2, 3	IRTF bolo
4796.....		1993 Apr 3, 5	IRTF bolo
2174.....		1993 Apr 4, 5	IRTF bolo
4295.....	β UMa	1993 Apr 6	IRTF bolo
6723.....	68 Oph	1993 Jul 26	IRTF bolo

^a “IRTF bolo” refers to the single-channel 2–30 μm facility bolometer system at the IRTF, and “Big Mac” to the NASA MSFC mid-infrared array camera.

extinction data, so we applied the weighted mean of the extinction coefficients from UT 1993 April 1, 2, and 3, which are the highest quality data sets. We did not obtain extinction data for the July data, and that photometry is uncorrected. In the July and 10.3 μm September uncorrected measurements, the targets and standards were located 0.2 air masses apart. Extinction corrections, if available, would have been $\sim 2\%$, smaller than statistical errors of $\gtrsim 3\%$ and absolute calibration errors (see below).

Tables 4 and 5 list resulting flux densities, measured with the IRTF bolometer and Big Mac, respectively, for the 10 sources. Quoted flux density errors include 1 σ statistical errors and absolute calibration uncertainties of $\pm 6\%$ at 2–12.5 μm and $\pm 10\%$ at 20 μm .

3. ANALYSIS

3.1. Photospheric Energy Distribution

To determine the amount of excess emission from dust in the total flux densities quoted in Tables 4 and 5, the photospheric energy level needs to be determined precisely. A simple approach would be to fit a blackbody to the near-

TABLE 3
FILTER BANDPASSES

λ_0 (μm)	$\Delta\lambda$ (FWHM) (μm)
Big Mac: ^a	
8.8.....	0.9
9.8.....	1.0
10.3.....	1.0
11.7.....	1.1
12.5.....	1.2
10.8 (N).....	5.3
IRTF bolometer: ^b	
2.2 (K).....	0.42
3.45 (L).....	1.05
4.80 (M).....	0.57
7.8.....	0.7
8.7.....	1.2
9.8.....	1.2
10.3.....	1.3
11.6.....	1.3
12.5.....	1.2
10.1 (N).....	5.1
20.0 (Q).....	9.0

^a From Telesco et al. 1988, TK, and C. M. Telesco 1991, private communication.

^b From IRTF Observer’s Manual 1986.

infrared fluxes. The photospheric spectra at mid-infrared wavelengths ($\sim 10 \mu\text{m}$) will be on their Rayleigh-Jeans tails, so at those wavelengths any blackbody at $T \geq 3000 \text{ K}$ would be a good model.

However, the photospheric spectral shape will start to deviate from a Rayleigh-Jeans tail at near-infrared (2–5 μm) and shorter wavelengths. Hence the photospheric fit in the near-infrared will depend on temperature, even though the shape at $\sim 10 \mu\text{m}$ will not. In addition, the photospheric spectrum conceivably deviates from a blackbody if a more realistic energy distribution is adopted. Kurucz (1992) computed model atmospheres for G, F, A, B, and O stars that included the effects of line opacities from almost 10^6 lines. The hydrogen lines of the Paschen series appear clearly in model spectra at 0.8–1.4 μm , and those of the Brackett series appear at 1.5–1.6 μm . The Paschen and Brackett discontinuities at 0.8 and 1.5 μm , respectively, will affect the near-infrared photospheric spectral shape. Continuous absorption by H^- will be significant at infrared wavelengths above 1.6 μm , and particularly significant in stars with $T < 7000 \text{ K}$. For hotter stars, the continuous absorption from the ionization of neutral hydrogen will predominate; absorption by free-free transitions will increase with wavelength, just as for H^- absorption.

In view of these effects, we decided to model the photospheric flux with synthetic spectra from the Kurucz (1992; R. L. Kurucz 1993, private communication) model atmospheres, instead of with featureless blackbody spectra. We used a database of model atmospheres and programs to generate synthetic spectra supplied by R. L. Kurucz (1993, private communication). In most cases we used models with solar composition (metallicity): $[Z/H] = 0.0$. To fit the effective temperature and surface gravity, which are the other two parameters needed to specify a Kurucz model spectrum, we tried various fits to visual and UV photometry. We normalized the Kurucz models to near-infrared K and L fluxes (with the exception of HR 10, for which there was no near-infrared photometry available), because if they are normalized at V , for instance, too much near-infrared photospheric flux results for some of the stars, beyond the upper limit of the observational uncertainties.

The discrepancy between near-infrared observations and Kurucz models fitted at V possibly arises from uncertainties in the absolute calibration of α Lyr, our primary photometric standard. The absolute calibration of α Lyr lies above a solar-metallicity Kurucz (1979) model fit at 5000 \AA , by 4%–8% in the near-infrared (Tokunaga 1986). A more recent model of α Lyr with less than solar metallicity ($[Z/H] = -0.5$; Kurucz 1991; Cohen et al. 1992) also lies below KLM photometric observations (Tokunaga 1986 and references therein) by factors of $\sim 5\%$ – 13% . This model is also lower ($\sim 1\%$ – 3%) than the α Lyr near-infrared flux densities compiled by Hanner & Tokunaga (1991). It is possible that α Lyr shows a near-infrared excess from very hot dust, as discussed by Blackwell et al. (1986), Cohen et al. (1992), and an anonymous referee. Leggett et al. (1986) and Bessell & Brett (1988) find that the near-infrared colors of other A0 stars are similar to those of α Lyr. Leggett et al. (1986) find that model emission from A stars at KLM is always lower than observations. Hence it is possible that the near-infrared excesses of other A stars are similar to the excess of α Lyr.

The calibration of sources without near-infrared excesses, against α Lyr, can yield apparent near-infrared deficits with

TABLE 4
 IRTF BOLOMETER PHOTOMETRY

λ_0 (μm) (1)	$F_{\nu}(\text{tot})$ (Jy) (2)	$F_{\nu}(\text{dust})$ (Jy) (3)	λ_0 (μm) (1)	$F_{\nu}(\text{tot})$ (Jy) (2)	$F_{\nu}(\text{dust})$ (Jy) (3)
68 Oph:			HR 4796A:		
2.20 (K).....	12.5 \pm 0.76	...	2.20	3.06 \pm 0.18	...
10.1 (N).....	0.853 \pm 0.066	0.134	3.45	1.32 \pm 0.080	...
21 LMi:			4.80	0.776 \pm 0.051	...
2.20	15.4 \pm 0.93	...	7.8	0.369 \pm 0.037	0.067
3.45	6.90 \pm 0.41	...	9.8	0.115 \pm 0.046	...
4.80	3.94 \pm 0.24	0.30	10.1 (N).....	0.270 \pm 0.026	0.087
7.8	1.54 \pm 0.10	...	10.3	0.233 \pm 0.024	0.057
8.7	1.26 \pm 0.088	...	11.6	0.225 \pm 0.070	0.086
9.8	1.00 \pm 0.067	...	12.5	0.253 \pm 0.027	0.133
10.1 (N).....	0.927 \pm 0.072	...	HR 2174A:		
10.3	0.882 \pm 0.062	...	2.20	4.36 \pm 0.27	...
11.6	0.794 \pm 0.058	0.132	3.45	2.00 \pm 0.13	...
12.5	0.561 \pm 0.054	...	4.80	1.07 \pm 0.078	...
20.0 (Q).....	0.348 \pm 0.048	0.122	7.8	0.650 \pm 0.094	0.231
σ Her:			10.1 (N).....	0.321 \pm 0.034	0.068
2.20	14.5 \pm 0.87	...	10.3	0.435 \pm 0.055	0.191
3.45	6.36 \pm 0.38	...	12.5	0.382 \pm 0.085	0.216
4.80	3.53 \pm 0.21	...	20.0 (Q).....	0.408 \pm 0.226	0.342
7.8	1.45 \pm 0.10	...	β UMa:		
8.7	1.09 \pm 0.076	...	2.20	71.6 \pm 4.3	...
9.8	1.02 \pm 0.072	0.132	3.45	31.2 \pm 1.9	...
10.1 (N).....	0.882 \pm 0.056	...	4.80	17.2 \pm 1.0	...
10.3	0.791 \pm 0.061	...	7.8	6.90 \pm 0.41	...
11.6	0.778 \pm 0.063	0.142	8.7	5.77 \pm 0.35	...
12.5	0.677 \pm 0.069	0.128	9.8	4.62 \pm 0.29	...
20.0 (Q).....	0.388 \pm 0.060	0.172	10.1 (N).....	4.20 \pm 0.26	...
γ Oph:			10.3	4.42 \pm 0.27	0.41
2.20	23.1 \pm 1.4	...	11.6	3.48 \pm 0.26	0.31
3.45	9.97 \pm 0.60	...	12.5	2.82 \pm 0.22	...
4.80	5.60 \pm 0.34	...	ζ Lep:		
7.8	2.04 \pm 0.13	...	2.20	27.7 \pm 1.9	...
8.7	1.80 \pm 0.12	...	3.45	12.4 \pm 0.9	...
9.8	1.56 \pm 0.13	...	4.80	6.85 \pm 0.49	...
10.1 (N).....	1.46 \pm 0.088	0.11	7.8	3.22 \pm 0.25	0.52
10.3	1.47 \pm 0.099	0.17	8.7	2.60 \pm 0.24	0.42
11.6	1.15 \pm 0.082	0.12	9.8	2.15 \pm 0.14	0.42
12.5	1.16 \pm 0.069	0.27	10.1 (N).....	2.06 \pm 0.13	0.43
20.0 (Q).....	0.561 \pm 0.098	0.212	10.3	2.03 \pm 0.18	0.46
			11.6	1.63 \pm 0.13	0.39
			12.5	0.94 \pm 0.14	...
			20.0 (Q).....	1.04 \pm 0.15	0.62

NOTE.—Photometric measurements with the 2–30 μm IRTF bolometer system; λ_0 gives the central filter wavelength (see Table 3), $F_{\nu}(\text{tot})$ is total flux density, and $F_{\nu}(\text{dust})$ is flux density after subtraction of a photospheric continuum.

respect to Kurucz models. We think that we saw this effect in some of our spectra when we first tried normalizing Kurucz models at V . In our new normalization at K or L , the photospheric flux is an adequate compromise fit to UV and UBV fluxes, within their errors. By normalizing at K or L we could still see whether there was any noticeable excess in the M flux, but we could not have detected any at K or L .

Observed UV spectrophotometric fluxes were obtained from Thompson et al. (1978), who estimated a 20% absolute calibration uncertainty. Visual photometry (UBV) is from Johnson et al. (1966), absolutely calibrated as described in Johnson (1965). We took the absolute calibration uncertainty of UBV Johnson photometry to be $\sim 3\%$.

We corrected the UV, visual, and near-infrared fluxes for interstellar reddening effects. The color excess E_{B-V} was estimated in most cases by comparing $B-V$ from Johnson et al. (1966) or Hoffleit & Jaschek (1982) with the intrinsic color $(B-V)_0$ of the star's spectral type (FitzGerald 1970); the spectral type was usually obtained from the SIMBAD

database. The Savage & Mathis (1979) extinction law was then used to obtain the wavelength-dependent extinction in magnitudes, A_{λ} .

The dereddening process will introduce errors arising mostly from uncertainties in the color excess E_{B-V} . The Savage & Mathis (1979) extinction law A_{λ}/E_{B-V} itself could also introduce errors; these are larger toward UV wavelengths (4%–8%) and negligible in the visual, as determined by comparing the extinction laws of Savage & Mathis (1979), Bless & Savage (1972), Nandy et al. (1976), and Code et al. (1976). In the near-infrared the dereddening correction is so small ($\sim 1\%$ at K and L and zero at M) that it will not add any significant errors on top of the calibration uncertainty of 6% (see above). At UV wavelengths, the calibration uncertainty is already so large (20%) that we can also neglect dereddening errors. The 1σ statistical errors quoted by Thompson et al. (1978) are typically $\sim 1\%$. The statistical errors in the visual are 1.4%–2.4% (Johnson et al. 1966). We conclude that in the UV the total error (including

TABLE 5
IRTF BIG MAC PHOTOMETRY

λ_0 (μm) (1)	$F_{\nu}(\text{tot})$ (Jy) (2)	$F_{\nu}(\text{dust})$ (Jy) (3)
HR 10:		
10.8 (N).....	0.153 ± 0.014	...
α PsA:		
8.8	19.2 ± 1.4	...
10.3	15.8 ± 1.0	...
10.8 (N).....	13.2 ± 0.81	...
11.7	12.7 ± 1.2	...
12.5	10.7 ± 1.6	...
ζ Lep:		
8.8	2.88 ± 0.26	0.75
9.8	2.00 ± 0.22	0.27
10.3	1.84 ± 0.14	0.27
10.8 (N).....	1.91 ± 0.12	0.48
11.7	1.56 ± 0.17	0.34
12.5	1.11 ± 0.16	...

NOTE.—Photometric measurements with the NASA MSFC bolometer array camera (Big Mac). See Table 4 for explanation of column headings; λ_0 is as in Table 3.

statistical, calibration, and dereddening uncertainties) is $\sim 20\%$; in the visual (UBV) it is 4% – 6% , and in the near-infrared we have already quoted it in Tables 4 and 5.

In Figure 1, we show the UV, UBV , and near-infrared photometry of ζ Lep, together with the best-fit Kurucz

(1992; R. L. Kurucz 1993, private communication) model spectrum for $T_{\text{eff}} = 9250$ K and $\log g = 4.0$. In the same figure we include our mid-infrared photometry to see how variations in the adopted photospheric continuum might affect the inferred mid-infrared excess. Figure 1 also shows two blackbody continua; as expected for the Rayleigh-Jeans approximation, they are indistinguishable beyond $3.5 \mu\text{m}$. However, these two blackbody spectra already differ from each other and from the Kurucz model by $\sim 6\%$ at $2.2 \mu\text{m}$ (K filter). A fit of the photosphere at K with a blackbody would thus have been unsatisfactory. The Kurucz model adequately matches all of the near-infrared data (K , L , and M filters). In addition, there is a perceptible difference between the blackbody and Kurucz model spectra at mid-infrared wavelengths; the former's fluxes are $\sim 2\%$ higher at $10 \mu\text{m}$, and nearly 5% higher at $12 \mu\text{m}$. Hence, a photospheric model with a blackbody continuum would underestimate the amount of excess at $\sim 10 \mu\text{m}$ by the above amounts. In stellar systems with weak infrared excesses, such as the ones in this survey, these differences are relevant; this is the main reason for our choosing the Kurucz models.

In Figures 2–10, we show similar fits of photospheric continua to the UV and UBV photometry of the sources in Table 1 besides ζ Lep (with the exception of HR 2174A, for which no UV spectrophotometry was available). Again, their near-infrared data (K , L , and M bandpasses in Tables 4 and 5) are used to further constrain photospheric fluxes.

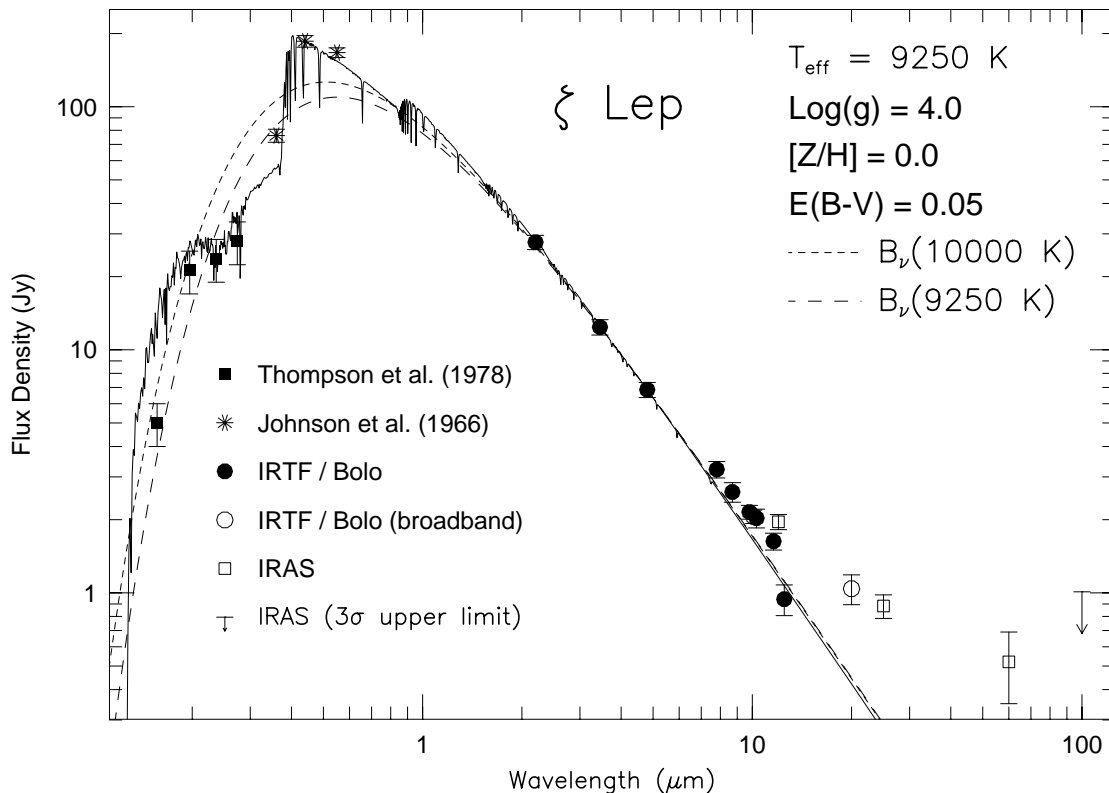


FIG. 1.—UV, visual, and infrared photometry of ζ Lep. A Kurucz (1992; R. L. Kurucz 1993, private communication) synthetic photospheric spectrum (solid line) was fitted in the near-infrared ($2\text{--}5 \mu\text{m}$) to our IRTF bolometer fluxes (filled circles) and further constrained by UV photometry from Thompson et al. (1978, filled squares) and visual (UBV , asterisks) photometry from Johnson et al. (1966). Error bars include 1σ statistical errors and absolute calibration errors, as explained in the text. The Kurucz model has $T_{\text{eff}} = 9250$ K, surface gravity $\log g = 4.0$, and solar metallicity ($[Z/H] = 0.0$). Two blackbody photospheric continua are also shown for comparison. We also show our measured broadband filter measurements at N and Q (open circles; the N measurement is more visible in Fig. 16, bottom), and $IRAS$ 12, 25, and $60 \mu\text{m}$ fluxes (open squares). The $IRAS$ $100 \mu\text{m}$ flux (arrow) is quoted as a 3σ upper limit in the $IRAS$ PSC. We use the same symbols for photometric points in Figures 2–10, unless otherwise indicated. $IRAS$ photometry is usually from the $IRAS$ PSC, except as noted; for ζ Lep 12, 25, and $60 \mu\text{m}$ $IRAS$ points are co-added photometry from Aumann & Probst (1991).

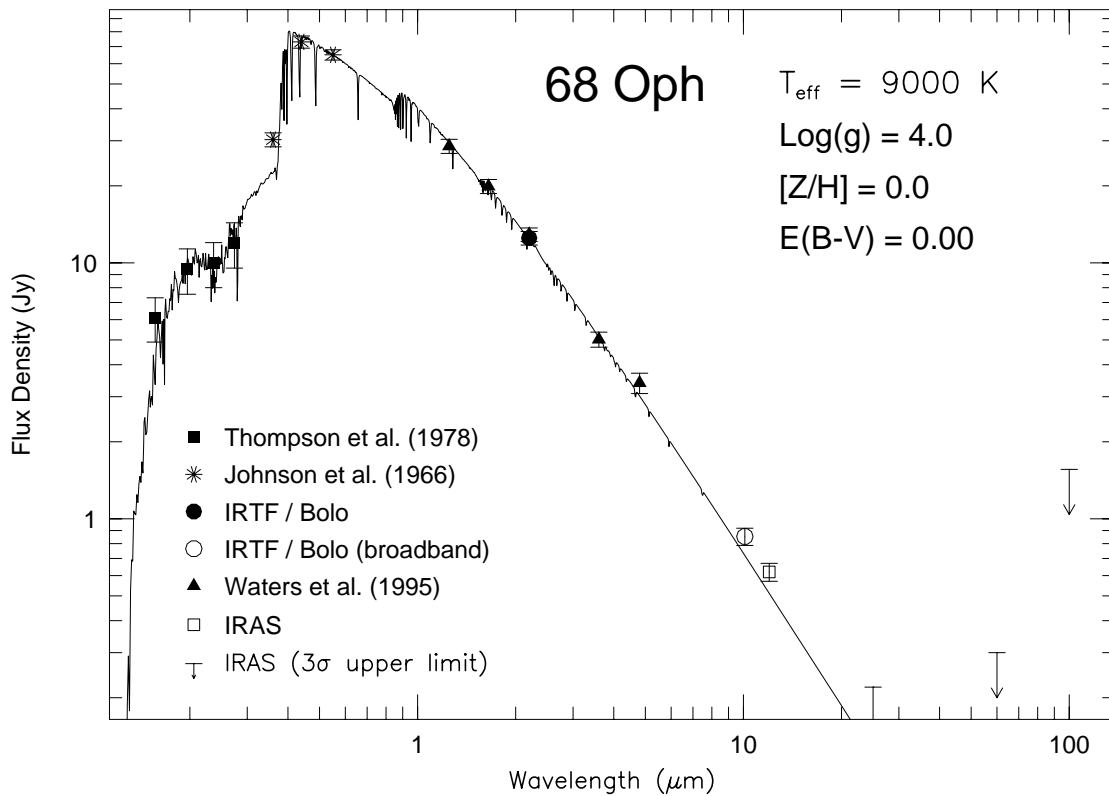


FIG. 2.—UV, visual, and infrared photometry of 68 Oph, and a Kurucz (1992; R. L. Kurucz 1993, private communication) synthetic photospheric spectrum; see Fig. 1 for details. Triangles are unreddened *JHKLM* photometry by Waters et al. (1995).

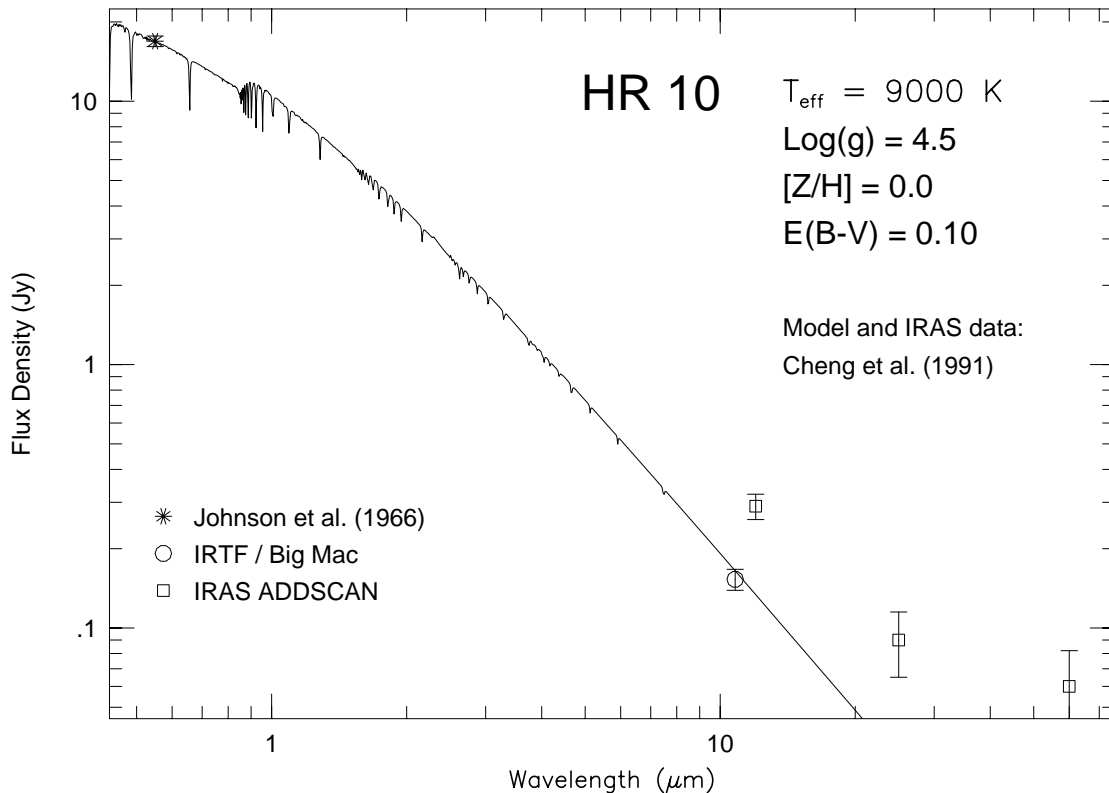


FIG. 3.—Visual (*V*) and infrared photometry of HR 10, and Kurucz photospheric model (with parameters derived by Cheng, Grady, & Bruhweiler 1991 from UV and visual fluxes; thus we only show *V*). *IRAS* fluxes were obtained by Cheng et al. with the ADDSCAN software.

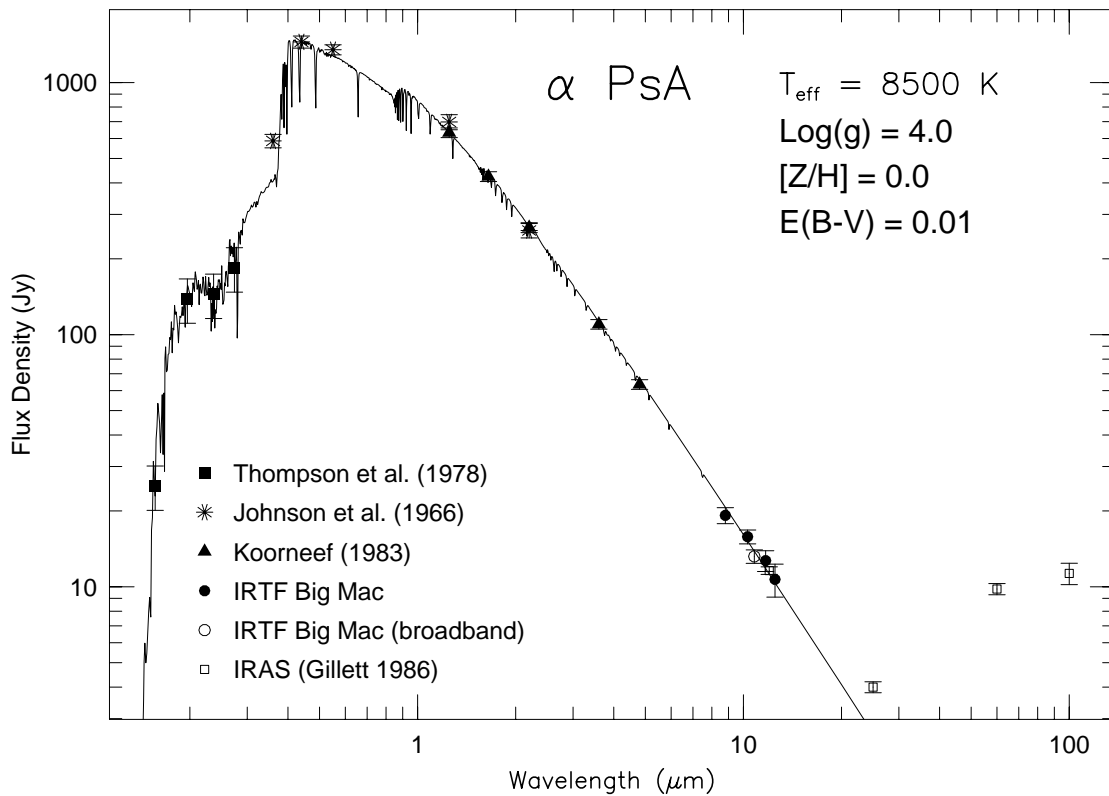


FIG. 4.—UV, visual, and infrared photometry of α PsA, and a Kurucz (1992; R. L. Kurucz 1993, private communication) synthetic photospheric spectrum. *IRAS* fluxes are from Gillett (1986). Near-infrared data are from Johnson et al. (1966, *asterisks*) and Koorneef (1983, *triangles*). The rest of the symbols are as explained in Fig. 1.

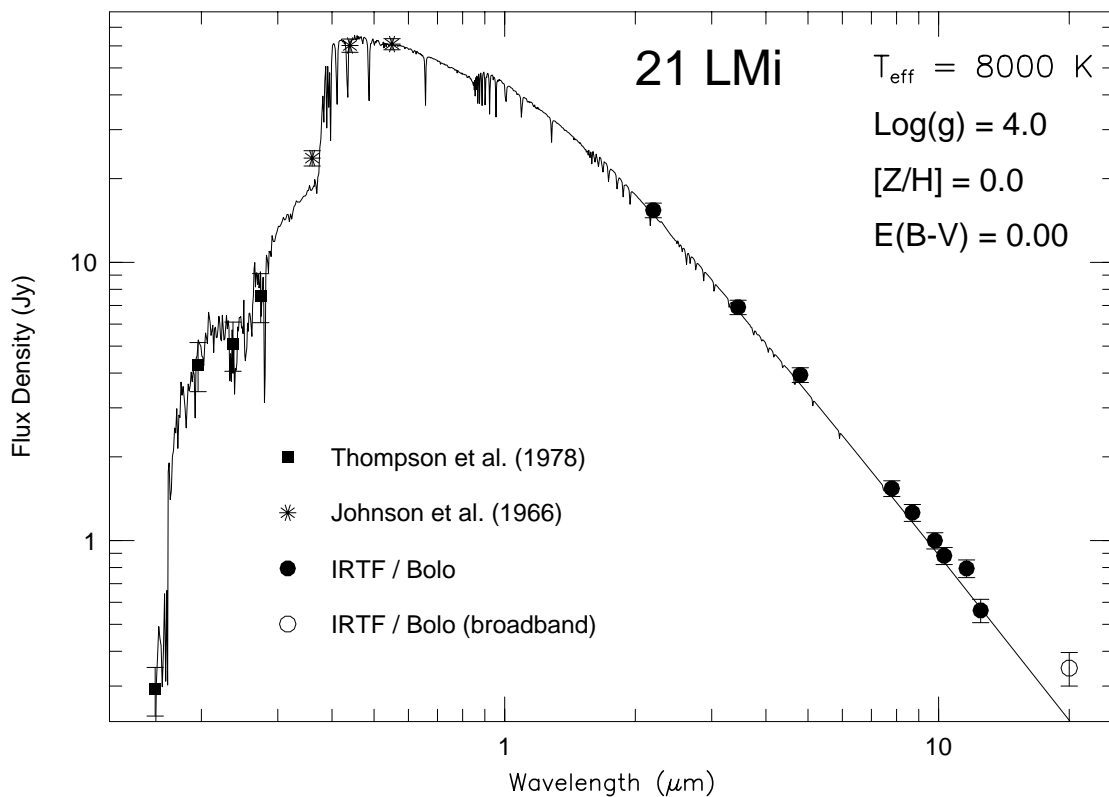


FIG. 5.—UV, visual, and infrared photometry of 21 LMi, and Kurucz photospheric model

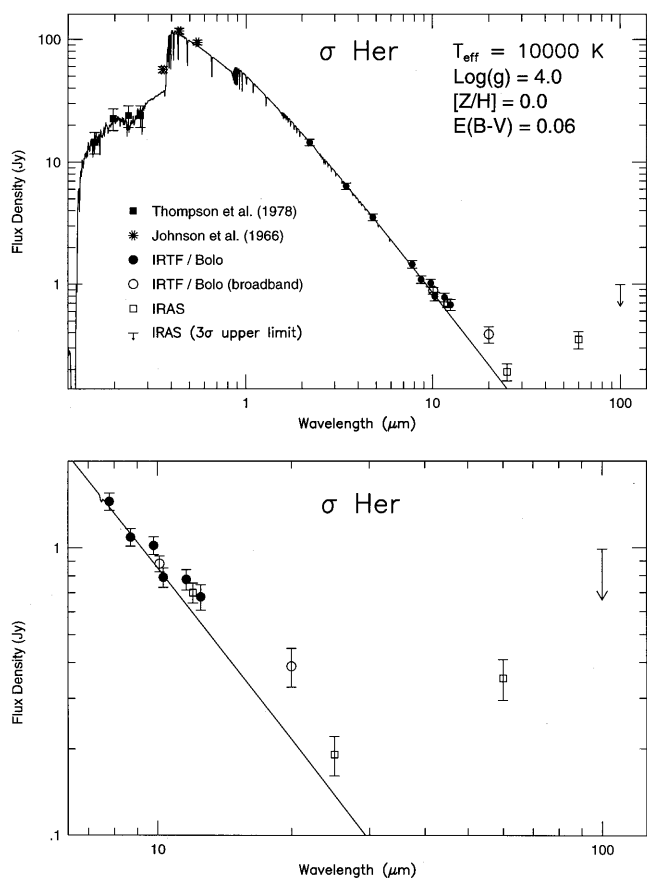


FIG. 6.—*Top*, UV, visual, and infrared photometry of σ Her, and Kurucz photospheric model; *bottom*, expanded plot of mid-infrared and IRAS photometry.

The relevance of near-infrared data in setting an upper limit to photospheric flux can be seen in Figures 1, 5, and 10 for ζ Lep, 21 LMi, and β UMa, respectively. In these cases the Kurucz model flux is slightly above the UV photometric fluxes. Lower effective temperatures would have improved the UV fits, but then the model fluxes would be above the near-infrared observations. We at first suspected a problem with the near-infrared data, but we have confirmed that it agrees with previous photometric data by other authors (discussed in § 3.2).

We compared our determination of stellar parameters (mainly effective temperature, since most models we used had $\log g \approx 4$) of β UMa, α PsA, and 68 Oph with those by Malagnini & Morossi (1990), Smalley & Dworetzky (1995), and Waters et al. (1995). For 68 Oph, Waters et al. (1995) fitted a Kurucz model with $T_{\text{eff}} = 9500$ K and $\log g = 4.0$ to optical and UV photometry. They used $E_{B-V} = 0.05$ to deredden their data. We used $E_{B-V} = 0$ and derived $T_{\text{eff}} = 9000$ K (Fig. 2), in reasonable agreement with Waters et al.'s model.

Malagnini & Morossi determined T_{eff} , E_{B-V} , and apparent angular diameters of field stars by fitting Kurucz models to visual spectrophotometry. Together with trigonometric parallaxes, these determinations allowed Malagnini & Morossi to locate the stars in the H-R diagram, where comparison with theoretical models then yielded surface gravities (and masses). In this way they derived for α PsA $T_{\text{eff}} = 9720$ K, $E_{B-V} = 0.10$, and $\log g = 4.43$. Their E_{B-V} is excessively high for this nearby star (7.0 pc distant). If this E_{B-V} is used to deredden α PsA's photometry, the UV fluxes and inferred T_{eff} will be relatively high for the star's spectral type (A3 V). We instead obtained $E_{B-V} = 0.01$, as explained earlier in this subsection, and our best-fit Kurucz model has

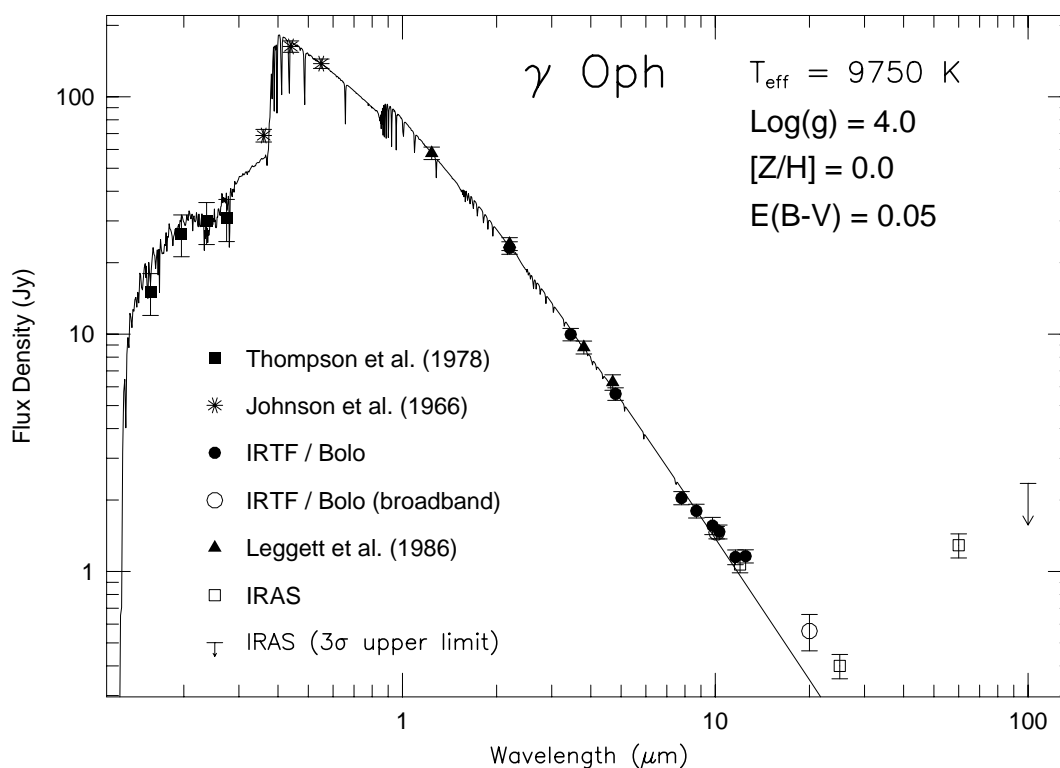


FIG. 7.—UV, visual, and infrared photometry of γ Oph, and Kurucz photospheric model. Triangles are near-infrared (*JKLM*) photometry by Leggett et al. (1986).

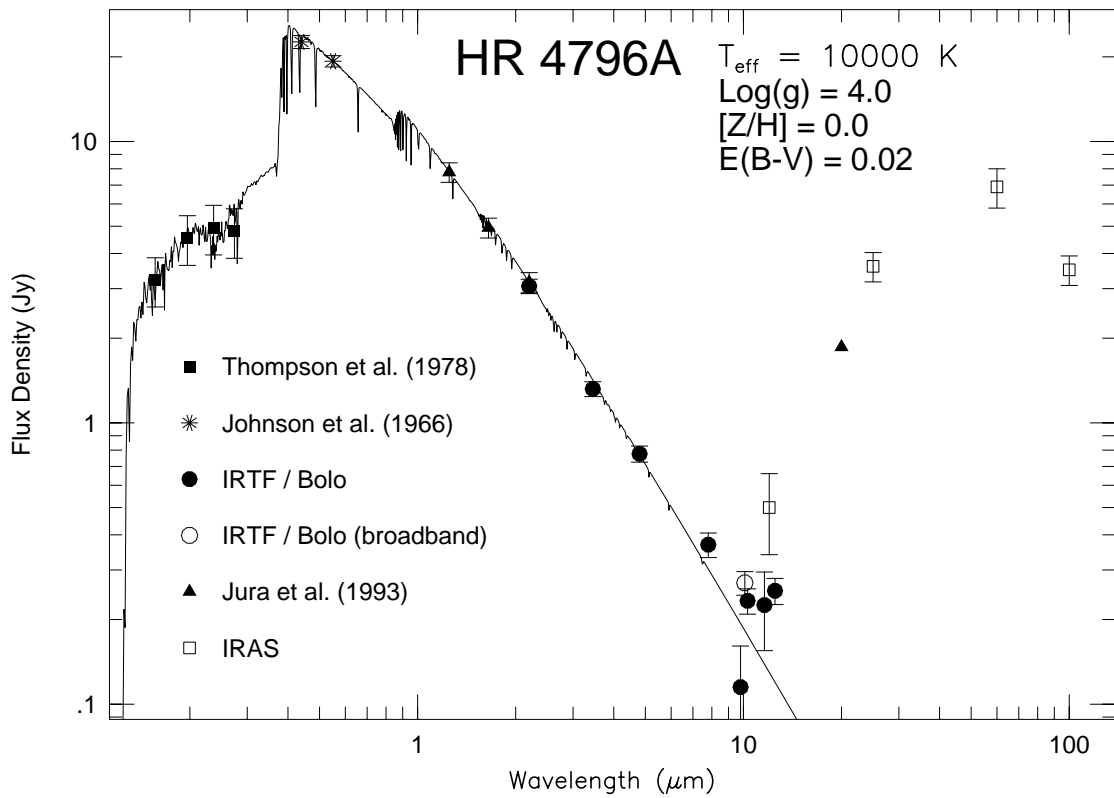


FIG. 8.—UV, visual, and infrared photometry of HR 4796A, and Kurucz photospheric model. Triangles are near-infrared (*JHK*) and $20.0 \mu\text{m}$ (*Q*) photometry by Jura et al. (1993).

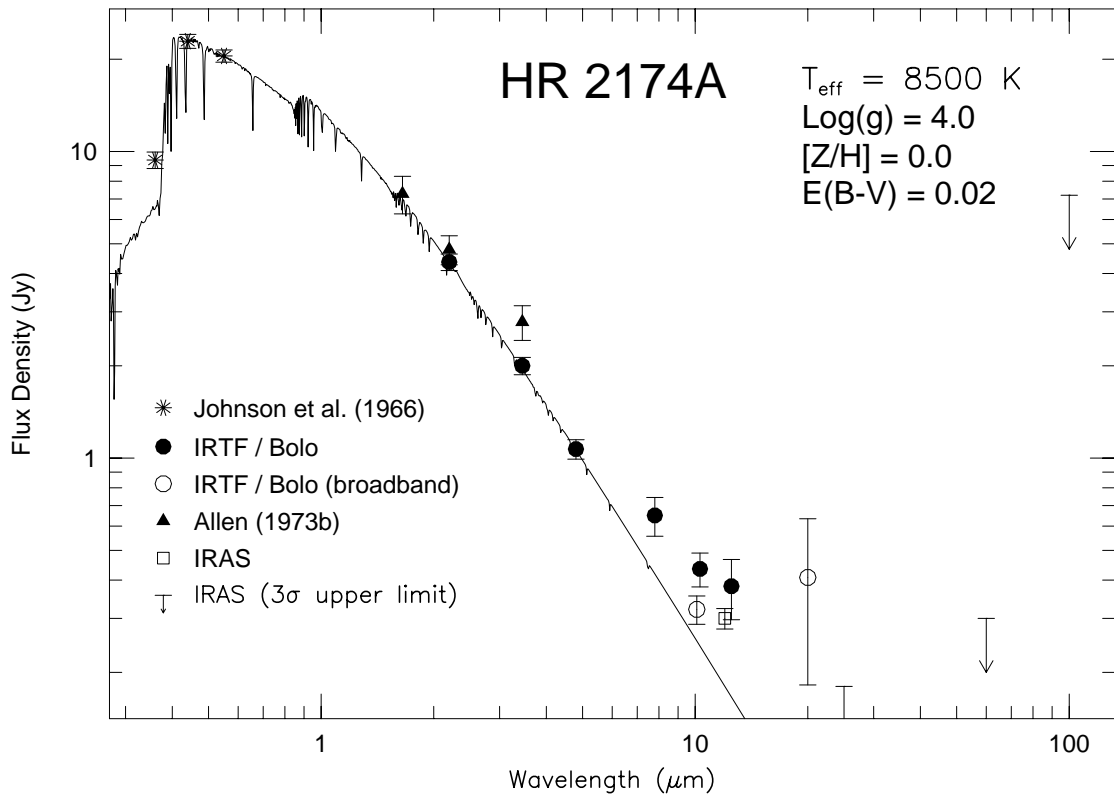


FIG. 9.—Visual (*UBV*) and infrared photometry of HR 2174A, and Kurucz photospheric model. UV fluxes were not available. We also plot near-infrared (*HKL*) photometry by Allen (1973, triangles).

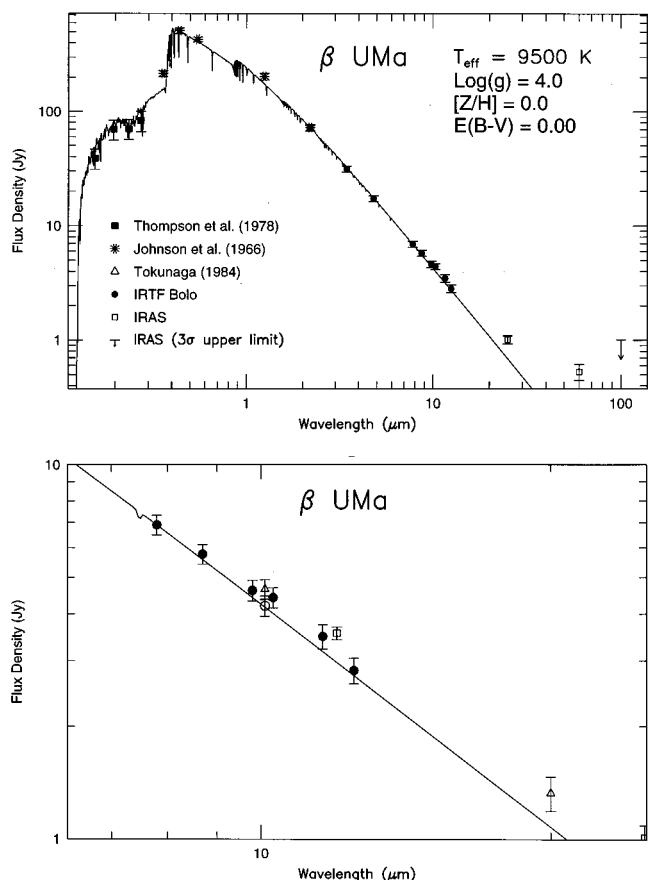


FIG. 10.—*Top*: UV, visual, and infrared photometry of β UMa, and Kurucz photospheric model. Also plotted are near-infrared (*JK*) photometry by Johnson et al. (1966, *asterisks*) and *Q* broadband photometry by Tokunaga (1984, *triangle*). For clarity, our broadband (*N*), *IRAS* 12 μ m, and Tokunaga’s broadband (*N*) measurements are not shown in this panel. *Bottom*: Detailed plot of mid-infrared (~ 7 –20 μ m) photometry, including data points not shown in the top panel.

$T_{\text{eff}} = 8500$ K and $\log g = 4.0$. Smalley & Dworetzky (1995) determined T_{eff} of α PsA from its apparent angular diameter and integrated flux (UV to infrared). They obtained $T_{\text{eff}} = 8760 \pm 310$ K, in good agreement with our value.

For β UMa we find $T_{\text{eff}} = 9500$ K and $\log g = 4.0$, whereas Malagnini & Morossi found $T_{\text{eff}} = 9700$ K and $\log g = 4.09$, quite in accordance with our values. β UMa’s color excess is very close to zero (either in our or in Malagnini & Morossi’s determination). Without the constraint of near-infrared photometry, our T_{eff} would have been lower.

Our model fits are within the uncertainties of UV photometry (Figs. 1–10), except for some cases at the shortest UV wavelength point (e.g., Fig. 1). In most other cases, the fit to UV data is good while the model flux is close to the near-infrared photometry. Cheng, Grady, & Bruhweiler (1991) determined the photospheric continuum of HR 10 with the same method we described here, so we simply use their result in Figure 3.

The photospheric temperatures T_{eff} we derived in Figures 1–10 are uncertain by about ± 250 K. Variations of this magnitude in T_{eff} yield Kurucz model fluxes still within the errors of UV and visual photometry in Figures 1–10.

3.2. Comparison with IRAS and Other Infrared Photometry

In order to verify the spectrophotometric data we have

obtained, and the photospheric energy distributions we inferred, we have searched the literature for previous infrared photometry of these sources (discussed in § 4.1 for each case). We also obtained the *IRAS* fluxes of these sources from the *IRAS* Point Source Catalog, Version 2 (1988, hereafter PSC). Depiction of our data together with *IRAS* and other mid- and near-infrared fluxes will not only allow us to put our mid-infrared photometry in perspective; we will also test for possible systematic errors in our flux levels, particularly in the near-infrared, where the photospheric levels were constrained. Comparing our fluxes with those in the larger *IRAS* beam can also give us some insight into the spatial extent of the circumstellar dust regions in these systems.

We corrected the *IRAS* PSC data for nonzero bandwidth effects (color correction). To apply the color correction, an assumption must be made about the spectral energy distribution (SED) of the source. In the literature on Vega-like stars, it is often assumed that the SED is that for a 10,000 K blackbody at the *IRAS* wavelengths. However, this is not necessarily the case for stars with infrared excesses of comparable magnitude to the photospheric flux. The *IRAS* Explanatory Supplement (1988, hereafter ES) tabulates color correction factors for blackbody and power-law forms for the SED, as a function of uncorrected PSC flux ratios. We obtained the correction factors for most of our sources, except as noted in § 4.1, assuming either form of SED in the ES. This choice of SED does not make a difference greater than $\sim 5\%$ in the correction factors from the ES.

4. RESULTS AND DISCUSSION

We subtracted the photospheric energy distributions in Figures 1–10 from our observed infrared flux densities, and the resulting excesses $F_{\nu}(\text{dust})$ are quoted in Tables 4 and 5 (col. [3]). If the fitted photospheric fluxes were slightly above our observed mid- or near-infrared fluxes (but still within the observational errors) then this is indicated by ellipsis dots in Tables 4 and 5 (col. [3]).

Figures 1–10 and Tables 4 and 5 show that none of the sources in our present study exhibit any significant excess in the near-infrared (1–5 μ m). At mid-infrared wavelengths we detected excess emission from some sources, but we did not detect the silicate emission feature in any of them. In this section we discuss salient features exhibited by our and other observers’ mid-infrared photometry, in the few instances where the latter is available. Our data generally constitute the first detailed mid-infrared SED determination for these sources, unless otherwise indicated.

4.1. Notes on Individual Sources and Models of Excess Emission

Some of the sources in our small-aperture photometric survey showed mid-infrared excesses, as discussed below. We attempted to fit their excesses with model emission from multitemperature circumstellar dust. We did not consider model disk geometries for the dust. There is no definitive observational evidence that the dust around our sources is distributed in disks. We instead considered spherical shell models of the dust around these sources. The parameters of the dust shell models are their inner and outer radial boundaries, r_1 and r_2 , and the exponent γ of radial dependence of volume number density of dust grains. That is, this density varies as $r^{-\gamma}$, where r is radial distance from the star. We modeled the flux from the portion of the dust shells

within our 5" observation beam. The Appendix gives more details on the shell models.

If we had considered disk instead of shell models, we would have obtained roughly the same results on mid-infrared model flux density, spatial extent (r_1 and r_2), and total surface area of dust grains (§ 4.3). A flat disk (with constant thickness perpendicular to the disk plane) and with density exponent $\gamma + 1$ will yield the same model results (in the above sense) as a shell with exponent γ . A wedge-shaped (flaring) disk with thickness proportional to r and with density exponent γ will yield the same results as a shell with the same γ (see Appendix).

In our models the radiative equilibrium temperatures of dust grains do not depend on particle sizes, because we assumed all dust grains to be blackbodies. It is possible that small grains, with wavelength-dependent emissivities, could yield better model fits to some of the excesses. However, we did not consider models of this kind, because of the low S/N of the data we are attempting to fit.

We next discuss the photometric data individually for all sources and the dust shell models for those sources with detected excesses.

68 Oph.—At mid-infrared wavelengths we obtained only one measurement through the broadband N filter. Other measurements were not possible, because of adverse atmospheric conditions. In any case, the N -filter point is consistent with the $IRAS$ 12 μm point (Fig. 2) in showing no mid-infrared excess. The $IRAS$ PSC 25, 60, and 100 μm points are quoted as 3 σ upper limits. Ratios of these uncertain fluxes are not very reliable descriptors of the SED, needed for color correction (§ 3.2). We color-corrected these data simply by assuming a 10^4 K blackbody SED, in order to compare them with similarly corrected data by Waters et al. (1995). They obtained co-added $IRAS$ photometry by using the $IRAS$ GYPSY system (Wesselius et al. 1992). Their measured 12 and 25 μm fluxes, and upper limits to 60 and 100 μm fluxes, agree within the plotted errors with the $IRAS$ PSC fluxes and upper limits in Figure 2. Waters et al. (1995) concluded that 68 Oph does not show significant excess at 12 and 25 μm from circumstellar dust. Waters et al. also obtained $JHKLM$ photometry of 68 Oph, plotted in Figure 2 (triangles). We added a 6% absolute calibration uncertainty to the statistical errors quoted by Waters et al. (1%–7%). These data agree quite well with our 2.2 μm measurement (Fig. 2) and with the fitted photospheric continuum.

HR 10.—Because of the faintness of this source (its $IRAS$ 12 μm flux is 0.29 Jy) and weather conditions, we could measure it only at 10.8 μm with the Big Mac broadband filter. From Figure 3 we immediately see that there is no excess at 10.8 μm in a $\sim 4''$ -diameter region around HR 10. The $IRAS$ 12 μm excess of ~ 0.16 Jy (from data by Cheng et al. 1991) thus originates in a more extended region. Cheng et al. argued that the $IRAS$ fluxes of this source were consistent with free-free emission, plus a small contribution from circumstellar dust. Free-free emission from plasma around the star would arise from within a few stellar radii. Our ground-based data do not confirm a circumstellar plasma or dust origin for this emission.

α PsA.—Our photometry at ~ 10 μm is consistent with the $IRAS$ 12 μm measurement, color-corrected by Gillett (1986), in showing no excess from warm dust (Fig. 4). All of our photometric points (Table 5) lie at the photospheric level, within the errors. This result is not surprising, given

that the $IRAS$ excess of α PsA can be modeled as arising from blackbody grains at temperatures of up to 100 K, located beyond 28 AU (Gillett 1986). Our observations sampled material within 2" from the star (or 14 AU at the distance of 7.0 pc to α PsA). Still, we searched for a weak excess at 10 μm because the $IRAS$ 12 μm flux lies somewhat above the model flux from blackbody grains (Fig. 1 of Gillett 1986).

21 LMi.—Aumann & Probst (1991) found that 21 LMi showed not only a [12] – [60] $IRAS$ excess, but also a K – [12] excess. They could not measure this star with a small aperture at N but encouraged observers to carry out this observation. We report that this star did not show significant excess in a 6" aperture at ~ 10 μm (see Fig. 5). Only the 11.6 μm point in our spectrum is above the continuum (at the 2 σ level). The $IRAS$ 12 μm excess is possibly due to contamination by another source in the $45'' \times 270''$ $IRAS$ beam used by Aumann & Probst (1991).

σ Her.—Figure 6 (top) shows our narrowband measurements of σ Her, together with UV and visual photometry, and our estimated continuum. The bottom panel shows in more detail our mid-infrared observations, including broadband (N and Q) and $IRAS$ fluxes. In Figure 11, we have

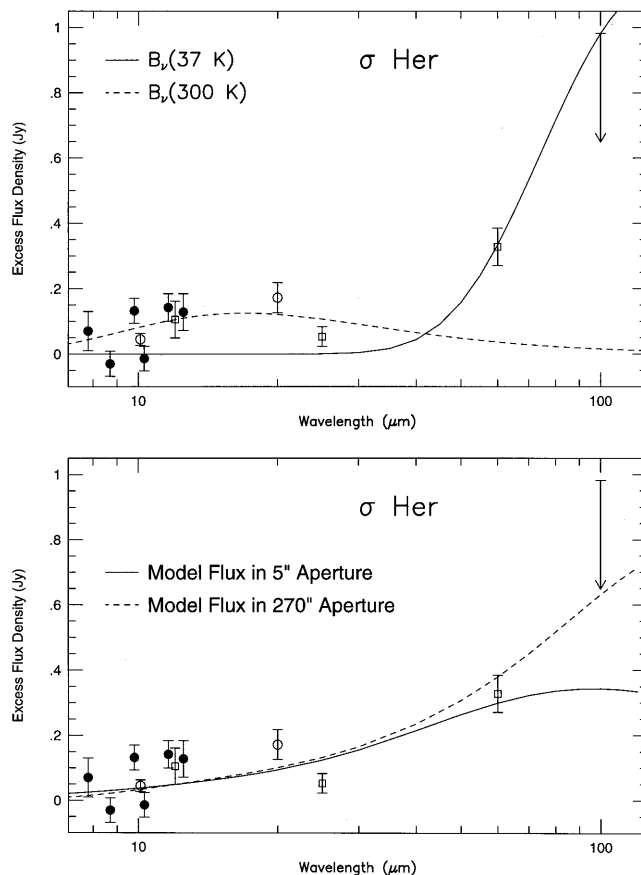


FIG. 11.—Excess fluxes of σ Her, after subtraction of the photospheric continuum in Fig. 6. Symbols for data points have the same meaning as in Fig. 6, but error bars here do not include absolute calibration uncertainties. *Top*: Two single-temperature blackbody dust models are shown. The solid line is a 37 K cold dust model intended to fit the far-infrared $IRAS$ data. The dashed line is a 300 K warm dust model to fit the ~ 12 –20 μm data. *Bottom*: Model flux from a shell of blackbody grains, extending from $r = 1$ to 2500 AU from the star, with number density decreasing as $r^{-0.9}$, as observed in a 5" beam (solid line) or in a 270" $IRAS$ -like beam (dashed line).

subtracted the photospheric continuum shown in Figure 6. Taken together, these data provide no evidence for an excess at wavelengths shorter than $10 \mu\text{m}$. On the other hand, the ground-based data at 11.6 and $12.5 \mu\text{m}$ agree closely with the *IRAS* data and may reveal an excess at $\sim 12 \mu\text{m}$ (at the 2σ level). At $20 \mu\text{m}$ and beyond, both *IRAS* data and ours indicate an excess increasing with wavelength. However, a single blackbody cannot account even for the *IRAS* excess fluxes alone. It seems as if the $12 \mu\text{m}$ excess arises from warmer dust than that responsible for excesses at $25 \mu\text{m}$ and longer wavelengths. In Figure 11 (*top*) we depict two blackbody continua to model cold and warm dust. A 300 K blackbody is a marginal fit to the ~ 12 – $25 \mu\text{m}$ data points, and a 37 K blackbody fits *IRAS* data points beyond $25 \mu\text{m}$. Oudmaijer et al. (1992) obtained a mean color temperature of 95 K from the 12 , 25 , 60 , and $100 \mu\text{m}$ *IRAS* fluxes. The agreement between ground-based and *IRAS* data points at $\sim 12 \mu\text{m}$ implies that warm dust is confined within $5''$ from the star. The small or zero excess flux at ~ 7 – $10 \mu\text{m}$ implies there is probably an inner “hole” in the dust region around σ Her.

We also attempted to fit the excess fluxes of σ Her with emission from a dust shell model (Fig. 11, *bottom*) of the kind described earlier in this section. Table 6 lists the model parameters r_1 , r_2 , and γ for σ Her and other sources with excesses. In the σ Her shell model the number density of blackbody grains decreases as $r^{-0.9}$. The shell extends from 1 to 2500 AU from the star. Two observing apertures ($5''$ and $270''$ diameter) were simulated to see the differences between ground-based and *IRAS* data. The $270''$ aperture size is comparable to the longest dimension of the various *IRAS* rectangular beams in the four *IRAS* bandpasses. The models were optimized by visual inspection of their fits to the data, but the uncertainty in the excess (or lack thereof) at wavelengths shorter than $12 \mu\text{m}$ prevents us from claiming that they are either unique or satisfactory fits. We can conclude from the models shown in Figure 11 that the excess of σ Her starting at $12 \mu\text{m}$ is not associated with a single blackbody, and even multitemperature distributions of blackbody grains are not an optimum fit to the data. It could be the case that a two-component disk or shell model fits the data. But the complexity of these models (see Backman, Gillett, & Witteborn 1992 for the case of β Pic) and the modest S/N of our data again prevent firm conclusions.

γ Oph.—Figure 7 shows photometry of γ Oph and its estimated continuum. It is difficult to make the case for an

excess at wavelengths $\leq 10 \mu\text{m}$. However, starting at $\sim 11 \mu\text{m}$ there is definite evidence of an excess roughly increasing with wavelength toward the far-infrared. It is significant that our 11.6 and $12.5 \mu\text{m}$ ground-based fluxes in a $5''$ aperture agree within the errors with the $12 \mu\text{m}$ *IRAS* flux. Such is also the case for our $20 \mu\text{m}$ measurement and the $25 \mu\text{m}$ *IRAS* flux. The dust region emitting at 12 and $25 \mu\text{m}$ must be confined to within $5''$ from the star (or $\sim 130 \text{ AU}$ at the distance of 26 pc to γ Oph).

We first attempted to fit the infrared excess fluxes (in Fig. 12) with a single-temperature blackbody function. It proved difficult to do this even for the *IRAS* data alone. A compromise fit was found with a blackbody at 65 K (not shown). Oudmaijer et al. (1992) obtained a mean *IRAS* color temperature of 80 K , quite in accordance with our value. The excess spectrum of γ Oph looks very similar to that of σ Her, discussed above. The color temperatures of Oudmaijer et al. are very similar in the two cases, and so should be the results of our model fits.

We next tried to fit the excess fluxes of γ Oph with model emission from a shell of blackbody grains (Fig. 12). We found that a density distribution $n(r) \propto r^{-0.8}$ for this shell produced a compromise fit. The shell extends from 1 to 2500 AU . The model is very similar to that of σ Her (Table 6). This model purported to fit the data at wavelengths $\geq 11 \mu\text{m}$. The model flux is from a $270''$ aperture (Fig. 12, *dashed line*), to approximate the size of an *IRAS* beam, as described above for the case of σ Her. We also modeled the flux in a $5''$ aperture (*solid line*) to represent ground-based data. Figure 12 shows that model flux in the two apertures is nearly identical at wavelengths $\leq 25 \mu\text{m}$, consistent with our earlier assessment that this flux is confined within $5''$.

HR 4796A.—*HR 4796* is a triple system in which we observed its component *HR 4796A* (A0 V). Figure 8 is the UV to far-IR spectrum of *HR 4796A*, together with its photospheric continuum. This figure summarizes in detail the infrared observations of *HR 4796A* obtained to date. The error bars include absolute calibration uncertainties of $\pm 6\%$ at 2 – $12.5 \mu\text{m}$ for ground-based data. The data by Jura et al. (1993) did not originally include absolute calibration errors, but we have added these in the plotted near-infrared points. The error bars of the *IRAS* data are as tabulated in the *IRAS* PSC. The $20.0 \mu\text{m}$ broadband (*Q* filter) flux of Jura et al. (1993) was quoted without uncertainty, but we estimate the absolute calibration error to be $\pm 10\%$. We subtracted the photospheric spectrum in Figure 8 from the observed fluxes, and the resulting excesses are shown in Figure 13, where the error bars include only statistical uncertainties and not absolute calibration errors. The practically null excess at $\sim 10 \mu\text{m}$ in the narrowband silicate filters is consistent, together with the *IRAS* points, with a featureless blackbody at $T = 110 \text{ K}$, which is the *IRAS* color temperature quoted by Jura (1991). The *IRAS* $12 \mu\text{m}$ point lies above the ground-based data. The reason could be that the wider *IRAS* filter passband samples some of the rising flux longward of $12 \mu\text{m}$ (Fig. 8). Alternatively, the *IRAS* $12 \mu\text{m}$ flux could be interpreted as consistent with ground-based data since it differs from them within only 1σ . The ground-based $20.0 \mu\text{m}$ and *IRAS* $25 \mu\text{m}$ points are consistent with emission from the 110 K blackbody described above. Therefore, the $20.0 \mu\text{m}$ and *IRAS* $25 \mu\text{m}$ fluxes arise from the same area. Jura et al. (1993) reached a similar conclusion and found that the $20 \mu\text{m}$ flux is confined within a 5.4 beam.

TABLE 6
MODELS OF SYSTEMS WITH EXCESSES

NAME	L_{dust}/L_* ^a	DUST SHELL MODELS ^b			Area ^c (cm^2)
		r_1 (AU)	r_2 (AU)	γ	
σ Her	6.6×10^{-5}	1	2500	−0.9	2×10^{28}
γ Oph	8.9×10^{-5}	1	2500	−0.8	4×10^{26}
<i>HR 2174A</i>	1.3×10^{-3}	0.5	2500	−1.5	4×10^{27}
β UMa	3.0×10^{-5}	1	2500	−1.8	1×10^{25}
ζ Lep	1.7×10^{-4}	0.5	1000	−1.6	9×10^{25}

^a Fractional dust luminosity.

^b Models of circumstellar shells of blackbody grains. Shells bounded by inner and outer radial distances from the star, r_1 and r_2 , respectively. Total volume number density of dust grains varies as r^{γ} .

^c Geometric cross-sectional area of all dust grains that would be observed in a $5''$ beam, in the shell models.

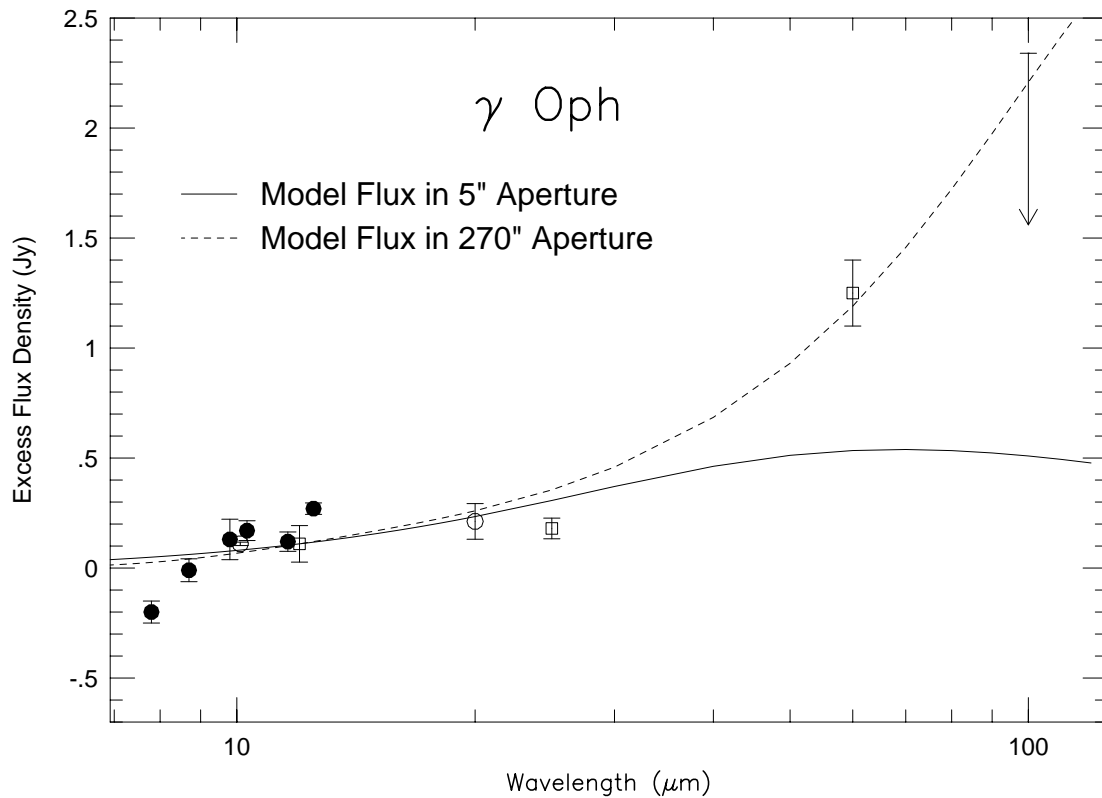


FIG. 12.—Excess fluxes of γ Oph after subtraction of the photospheric continuum in Fig. 7; we use a similar key to data point symbols. Error bars do not include absolute calibration uncertainties. We show the model flux from a shell of blackbody grains extending from 1 to 2500 AU with number density decreasing as $r^{-0.8}$ AU. Solid line, 5" beam; dashed line, 270" IRAS-like beam.

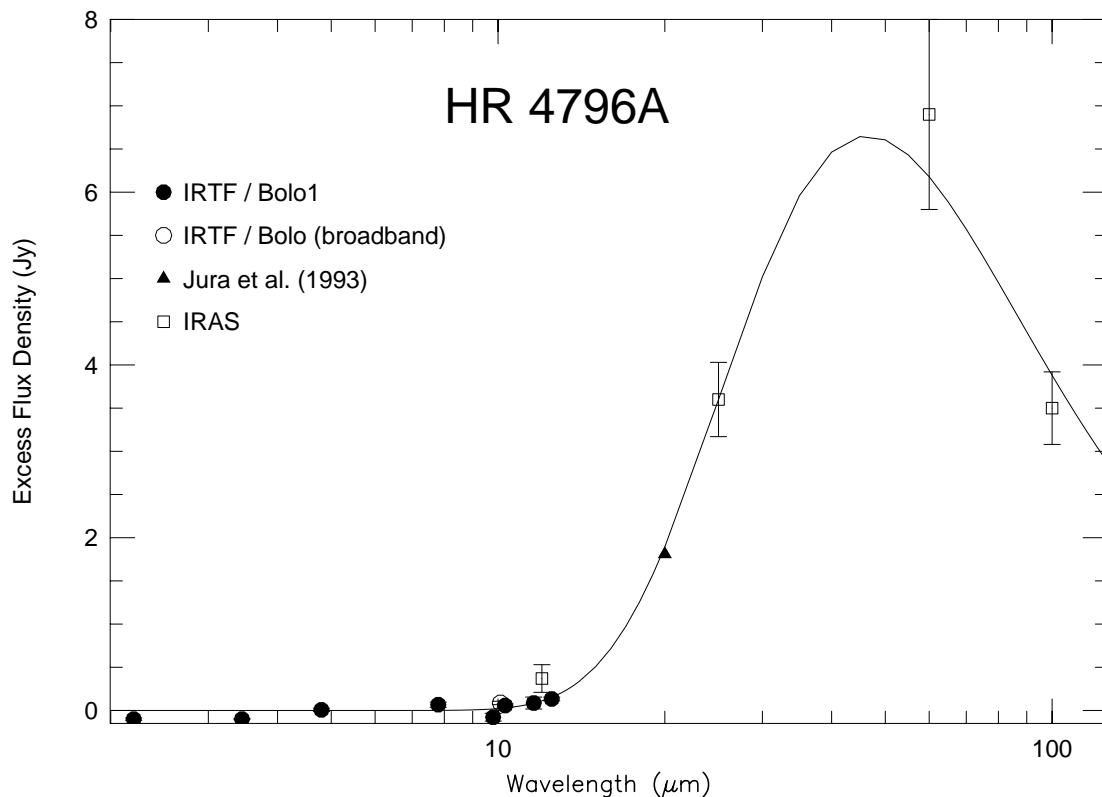


FIG. 13.—Excess fluxes of HR 4796A after subtraction of the photospheric continuum in Fig. 8; we use a similar key to data point symbols. Error bars do not include absolute calibration uncertainties. We show the model flux from a blackbody at 110 K, which was found by Jura et al. (1993) to be a good fit to the IRAS and Q photometry.

The absence of dust hotter than ~ 110 K around HR 4796A led Jura et al. (1993, 1995) to conclude that there is an inner hole of radius greater than 40 AU in this system. The dust around HR 4796A could be distributed in a disk or shell, extending from $r_1 > 40$ AU, with very steep radial decrease of volume number density (large negative γ exponent). The material at r_1 would dominate the excess SED, which would be that of the single-temperature blackbody already described. The grains located beyond 40 AU have radii greater than $3 \mu\text{m}$; smaller grains would be ejected by radiation pressure (Jura et al. 1995). These authors proposed that dust grains closer than 40 AU from the star coalesced into macroscopic objects, possibly planets. Grains beyond 40 AU must also have undergone coalescence, since they are larger than typical interstellar grains (Jura et al. 1995).

In the HR 4796 stellar system, two of its components, HR 4796A and HR 4796B (\sim M4 pre-main sequence), form a physical pair (Jura et al. 1993). The estimated age of HR 4796B (and therefore also of HR 4796A) is $\sim (8 \pm 2) \times 10^6$ yr (Stauffer, Hartmann, & Barrado y Navascues 1995). This age estimate places the HR 4796A circumstellar system in an earlier evolutionary stage than those of β Pic or other main-sequence stars.

HR 2174A.—HR 2174 is a 29" binary system; observations here are of the brighter component, HR 2174A. *IRAS* PSC data in Figure 9 (quoted as 3σ upper limits at 25, 60, and $100 \mu\text{m}$) were corrected using a 10^4 K blackbody energy distribution, just as in the case of 68 Oph. The photospheric continuum (Fig. 9) was estimated by fitting a Kurucz model to visual and near-infrared data since no UV fluxes were available. If there were a near-infrared excess,

we would miss it with this method. But the slope from our *K*, *L*, and *M* photometry (Fig. 9) is consistent with a purely photospheric spectrum in the near-infrared. We compared these fluxes with *H*, *K*, and *L* photometry by Allen (1973), who used an unspecified aperture. His *L* measurement is considerably higher than ours (nearly 40%). Allen quoted that photometry with high statistical uncertainties of 0.1 mag. On the other hand, we measured HR 2174A on two nights, so we believe our near-infrared measurements to be much more reliable. If one fitted the photospheric continuum at Allen's fluxes (Fig. 9), then one would infer a photospheric temperature below 8000 K, inconsistent with this star's spectral type (A3 V).

Despite the faintness of this source, we detected an excess at $10 \mu\text{m}$. The uncertainty of our ~ 10 – $20 \mu\text{m}$ data is high, but within the errors the 12.5 and $20.0 \mu\text{m}$ points agree with the 12 and $25 \mu\text{m}$ *IRAS* points, respectively. The $7.8 \mu\text{m}$ flux is considerably above the continuum, thus suggesting that very warm dust is around HR 2174A. In Figure 14, we subtracted the photospheric continuum to obtain the excess spectrum. Neither the *IRAS* excesses alone nor ours can be fitted with a single-temperature blackbody. The excess emission is more likely from multitemperature dust. The 12, 25, and $60 \mu\text{m}$ *IRAS* data can be marginally fitted with model flux from a shell of blackbody grains extending from 1 to 2500 AU, with volume number density $\propto r^{-1.2}$. A $270''$ aperture was used for the model fluxes (Fig. 14, *dashed line*). A better fit to the $\sim 10 \mu\text{m}$ narrowband measurements comes from grains in a similar shell extending from 0.5 to 2500 AU from the star, with more steeply decreasing number density $\propto r^{-1.5}$ (Table 6). This model spectrum (Fig. 14, *solid line*) is from a $5''$ aperture. The conclusion that

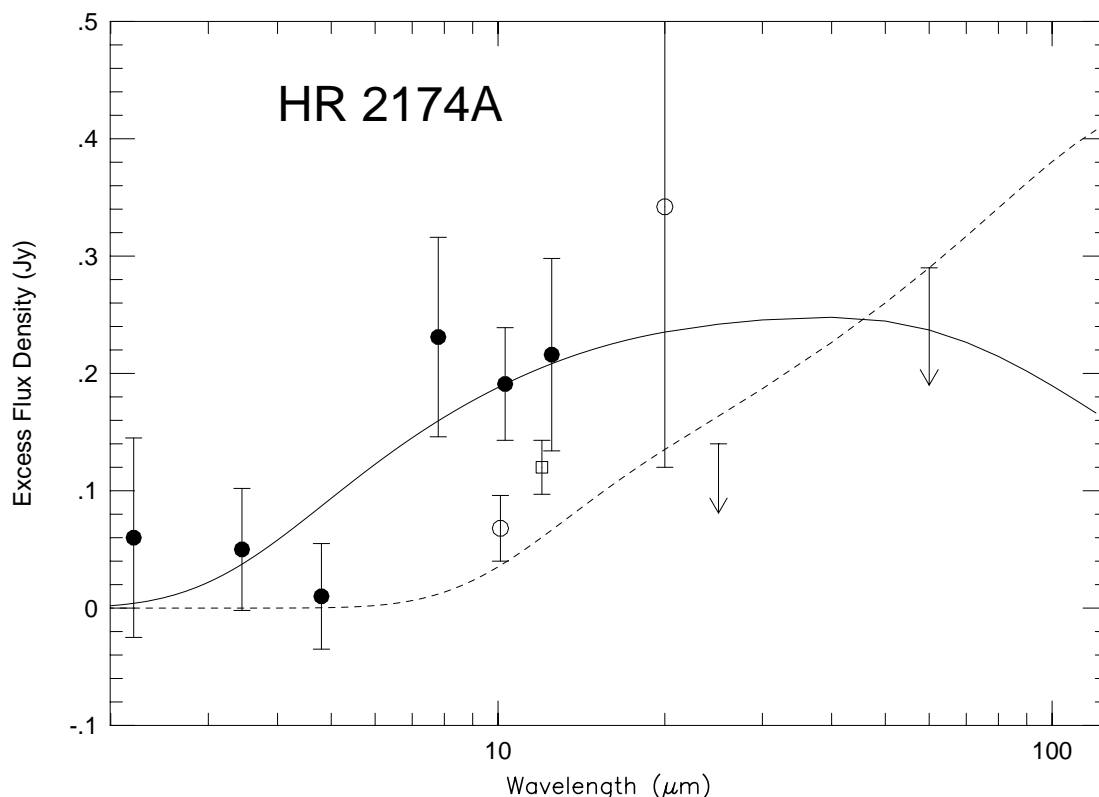


FIG. 14.—Excess fluxes of HR 2174A after subtraction of the photospheric continuum in Fig. 9. *Solid line*, model flux in a $5''$ aperture from a shell of blackbody grains, extending from 0.5 AU to 2500 AU, and with number density $\propto r^{-1.5}$; *dashed line*, model flux in a $270''$ *IRAS*-like beam from a shell extending from 1 to 2500 AU, with a flatter density distribution $\propto r^{-1.2}$.

we draw from these models is that a substantial quantity of dust grains might be located very close to HR 2174A in order to produce the high excess flux at wavelengths as short as $7.8 \mu\text{m}$.

β UMa.—From Figure 10 (*top*) we see that our near-infrared measurements are in close agreement with *J* and *K* photometry by Johnson et al. (1966), and so is our photospheric continuum flux level. Our mid-infrared photometry is shown in detail in the bottom panel. In the same figure we also plot our measurements in the broadband *N* filter, the *N* and *Q* measurements by Tokunaga (1984), and the *IRAS* PSC $12 \mu\text{m}$ point. Figure 10 shows that our 10.3 and $11.6 \mu\text{m}$ points, and the broadband *N* point of Tokunaga, indicate a small excess between 10 and $12 \mu\text{m}$, which reappears again at $\sim 20 \mu\text{m}$. The *IRAS* 12 and $25 \mu\text{m}$ data agree with the ground-based photometry, within the errors. Although β UMa's mid-infrared fluxes seem to be as close to the continuum as those of 21 LMi, the latter's spectrum showed only one point ($11.6 \mu\text{m}$) above the continuum. β UMa's spectrum could plausibly exhibit a very weak silicate emission feature, but this inference must be made with great caution due to the smallness of the excess. Figure 15 shows the possible excess fluxes of β UMa, including *IRAS* data.

A single blackbody cannot fit all of the *IRAS* excess fluxes. The 7 – $12 \mu\text{m}$ ground-based data cannot be fitted with a blackbody at $T \sim 500$ K, because the $10 \mu\text{m}$ peak of the emission is too narrow. We attempted to fit the data in Figure 15 (*top*) with emission from a shell model, as described above. The parameters of the model are $r_1 = 1$ AU, $r_2 = 2500$ AU, and $\gamma = -1.8$ (Table 6). Figure 15 (*top*) shows model emission spectra from within $5''$ and $270''$ beams. These models are a compromise fit to ground-based and *IRAS* data. The latter are not fitted well at 60 or $100 \mu\text{m}$.

We could speculate on the presence of a weak $10 \mu\text{m}$ silicate feature, superposed on a broader continuum, in the excess spectrum of β UMa. The 7.8 , 12.5 , and $20.0 \mu\text{m}$ ground-based fluxes are well fitted by a 180 K blackbody (Fig. 15, *bottom*). We take it as the underlying dust continuum. Presumably the grains producing the silicate feature would be very small (radius less than $1 \mu\text{m}$) in order for most of the excess $10 \mu\text{m}$ flux to arise from silicate emission. Only $\sim 5\%$ of the $10 \mu\text{m}$ flux would arise from blackbody grains at 180 K.

ζ Lep.—This star exhibits the largest $10 \mu\text{m}$ excess of any in our survey (Fig. 1). Aumann & Probst (1991) had found that only ζ Lep and β Pic, out of a sample of 55 A, F, G, and K stars with an *IRAS* $12 \mu\text{m}$ excess greater than 0.3 mag, exhibited $10 \mu\text{m}$ (*N*) excesses in ground-based, small-aperture measurements. From *K* and *N* measurements by Aumann & Probst (1991) we estimated that the $\sim 10 \mu\text{m}$ excess of ζ Lep was ~ 0.28 Jy, about 13% of its total flux. Tables 4 and 5 (col. [3]) show that this estimate is quite consistent with that from our $10 \mu\text{m}$ photometry and the Kurucz model in Figure 1. Figure 16 (*top*) shows, in addition to our photometry, near-infrared (*JHKL*) dereddened measurements by Aumann & Probst (1991) (we applied the dereddening and absolute calibration ourselves) and *IRAS* color-corrected fluxes. The near-infrared fluxes of Aumann & Probst (1991) are $\sim 15\%$ higher than ours. This is mainly because the photometry of Aumann & Probst mimics that in a $2'$ aperture, much more extended than our $5''$ beam. The former aperture was used as an analog of the $12 \mu\text{m}$ *IRAS* beam and can include field stars in the vicinity of the source.

Still, there is marginal agreement within the total (statistical and calibration) errors between our and Aumann & Probst's photometry. We also compared the two sets of mid-infrared measurements of ζ Lep obtained with Big Mac (1992 September) and the IRTF bolometer ("Bolo") (1993 April) at the IRTF (see Fig. 16, *bottom*). The narrowband filter sets of the two instruments are not identical. Therefore we did not combine the two data sets, in order to avoid spectral distortions. Both Big Mac and IRTF bolometer spectrophotometry suggest a relative flux increase at $\sim 11 \mu\text{m}$ with respect to points at ~ 10 or $12 \mu\text{m}$. The data at ~ 8 – $9 \mu\text{m}$ also seem relatively high in both data sets (Fig. 16, *bottom*) with respect to the underlying continuum (Fig. 16, *top*) and $10 \mu\text{m}$ data. This can be seen more clearly in Figure 17, which shows the photometry of ζ Lep after subtraction of the photospheric continuum. In Figures 16 (*top*) and 17, for clarity we have not plotted the Big Mac photometry. The two data sets are consistent, yet the IRTF bolometer photometry was obtained under better atmospheric conditions, so we rely on the latter for further comments. The shape of the spectrum we described, and the fact that the $20 \mu\text{m}$ excess (Fig. 17) lies above the $10 \mu\text{m}$ one could plausibly suggest the presence of silicate emission, which typically shows two peaks, at 10 and $20 \mu\text{m}$. The high excess flux level at $7.8 \mu\text{m}$ (Fig. 17) could arise from very hot grains.

We modeled the excess of ζ Lep as from a dust shell (Table 6) extending from 0.5 to 1000 AU from ζ Lep. The number density of grains decreases steeply with radial distance r , as $r^{-1.6}$. This model thus relies on hot grains to produce some of the short-wavelength ($\sim 8 \mu\text{m}$) excess. In Figure 17, we show the model flux. The fit to *IRAS* data (or to ours) is marginal, but much better than what any single-temperature blackbody could achieve. We modeled the flux in two apertures ($5''$ and $270''$; see Fig. 17) to simulate our small aperture and the *IRAS* one, respectively. We see that none of the models can reproduce the slope at 7 – $10 \mu\text{m}$ together with longer wavelength points. We note that our $20 \mu\text{m}$ point and the $25 \mu\text{m}$ *IRAS* one agree closely. On the other hand, the $12 \mu\text{m}$ *IRAS* point is higher than our small-aperture data, although within the absolute calibration uncertainties (plotted in Fig. 1) the disagreement is probably not significant. We found the same relations for the HR 4796A data (discussed above).

4.2. Fractional Dust Luminosity

A useful parameter to characterize circumstellar dust systems is the fractional dust luminosity, L_{dust}/L_* . It is the ratio of integrated excess flux emitted from dust, $\int_0^\infty dv F_\nu(\text{dust})$, to integrated flux emitted from the star alone, in the absence of circumstellar material, $\int_0^\infty dv F_\nu(\text{phot})$. Values of $F_\nu(\text{dust})$ for our sources are listed in Tables 4 and 5 (col. [3]). At *IRAS* wavelengths, $F_\nu(\text{dust})$ values are the *IRAS* flux densities (Figs. 1–10) minus $F_\nu(\text{phot})$. Values of $F_\nu(\text{phot})$ are those of the dereddened photospheric models plotted in Figures 1–10.

Backman & Gillett (1987) argued that a mean optical depth of circumstellar dust grains is given by the fractional dust luminosity L_{dust}/L_* . The fractional dust luminosity would exactly equal the optical depth for a spherical dust shell configuration. In the case of a flaring disk, the optical depth along the disk plane would equal the fractional dust luminosity times $4\pi/\Omega$, where Ω is the solid angle subtended by the disk as seen from the star (D. Backman 1994, private

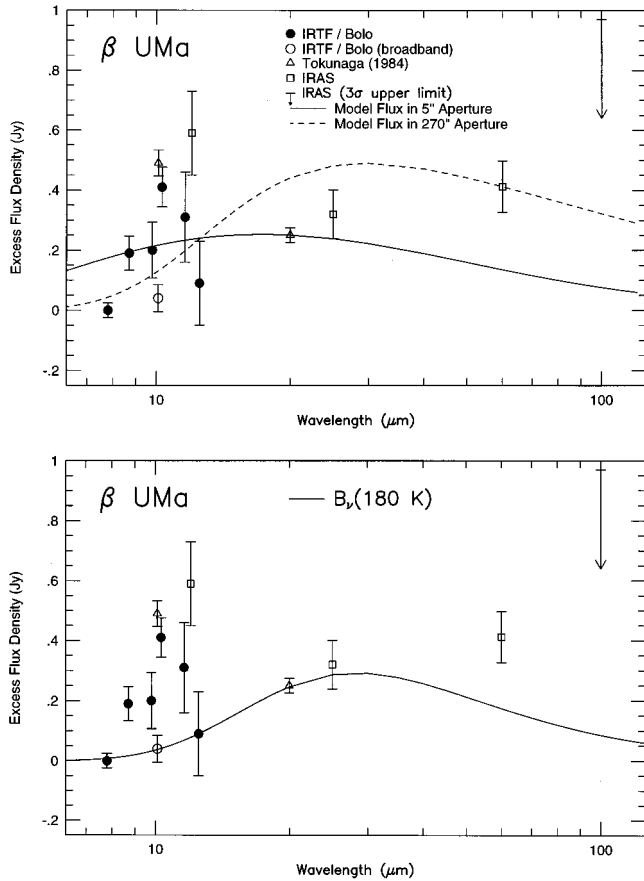


FIG. 15.—*Top*: Excess fluxes of β UMa after subtraction of the photospheric continuum in Fig. 10. *Solid line*, model flux in a 5" aperture from a shell of blackbody grains, extending from 1 to 2500 AU, and with number density $\propto r^{-1.8}$; *dashed line*, similar model flux in a 270" IRAS-like beam. *Bottom*: A 180 K blackbody is fitted to the 7.8 and 12.5 μm excess fluxes, to investigate whether emission features (such as from silicates) are superposed on this dust continuum.

communication). The fractional dust luminosity is a useful parameter because it allows comparison of dust properties of different stars, irrespective of the stellar characteristics. That is, Aumann (1985) and Sadakane & Nishida (1986) showed that the large relative number of A and B stars with dust detections was partly a stellar luminosity selection effect. The optical depth as defined above can eliminate this bias.

The fractional dust luminosities of our measured sources can let us place the properties of their circumstellar dust regions in perspective with other, comparable systems. Although 25% of A-type main-sequence stars have $L_{\text{dust}}/L_{*} > 5 \times 10^{-6}$ (Backman & Gillett 1987), only a fraction, $\sim 2 \times 10^{-3}$, have $L_{\text{dust}}/L_{*} > 10^{-3}$ (Jura et al. 1993). Examples of main-sequence stars with $L_{\text{dust}}/L_{*} > 10^{-3}$ are 49 Ceti, β Pic, HR 4796A, 51 Oph, and HD 98800 (Jura et al. 1993; Zuckerman & Becklin 1993), as determined from previous near-infrared and IRAS photometry.

We computed the fractional dust luminosities L_{dust}/L_{*} of sources in our small-aperture photometry survey that exhibited excess emission at 10 μm . These sources are σ Her, γ Oph, HR 2174A, β UMa, and ζ Lep. Jura (1991) computed $L_{\text{dust}}/L_{*} \sim 5 \times 10^{-3}$ for HR 4796A based on IRAS data. The bulk of the excess of HR 4796A is at IRAS wavelengths (Fig. 13). For the rest of our selected sources, Table 6 lists

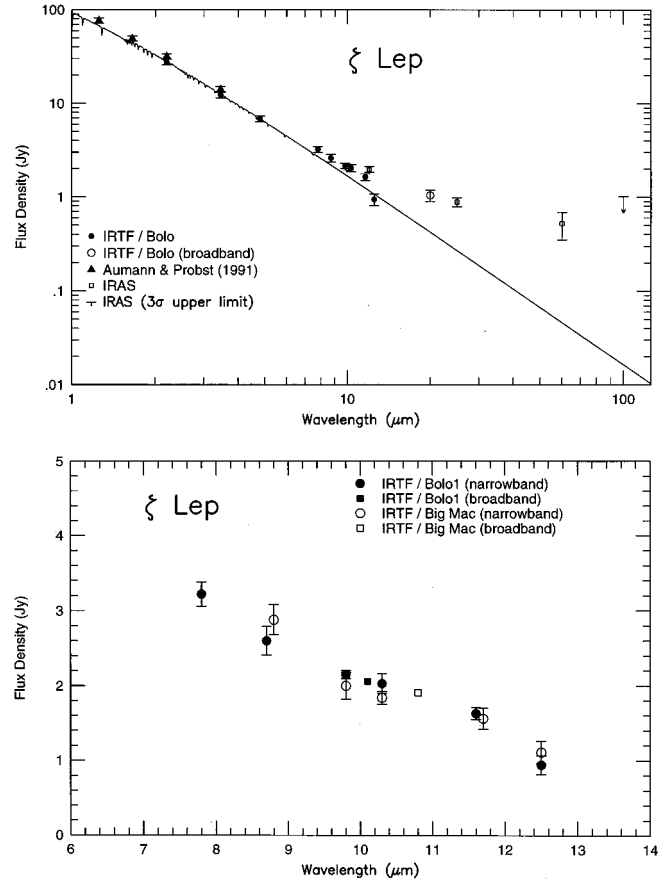


FIG. 16.—*Top*: Expanded plot of the infrared fluxes of ζ Lep. In addition, we include near-infrared (JHKL) photometry by Aumann & Probst (1991, *triangles*), summed over a 2' field of view to mimic the 45" \times 270" IRAS beam. We included a 6% absolute calibration uncertainty in the plotted error bars of this JHKL photometry. Big Mac fluxes are not shown for clarity. *Bottom*: Comparison of ζ Lep IRTF mid-infrared photometry obtained with Big Mac (*open symbols*) and the IRTF bolometer (*filled symbols*). Error bars do not include absolute calibration uncertainties; error bars of broadband (N) fluxes (*squares*) are the same size as the symbols shown.

their L_{dust}/L_{*} , which range from 3.0×10^{-5} (for β UMa) to 1.3×10^{-3} (for HR 2174A). These values confirm that the excesses of these sources are moderate. β UMa is a member of the Ursa Major Stream, and its inferred age ($\sim 2.7 \times 10^8$ yr) corresponds roughly to the era of heavy bombardment and planet construction in our solar system (Witteborn et al. 1982). The largest values of L_{dust}/L_{*} ($> 10^{-3}$) can be related to the presence of large quantities of circumstellar dust in the youngest systems or to infrared excesses from hot dust. The star 51 Oph has a large fractional dust luminosity, namely, $L_{\text{dust}}/L_{*} \sim 4 \times 10^{-2}$ (Zuckerman & Becklin 1993) due to its prominent near-infrared excess from ~ 1000 K dust (Waters, Coté, & Geballe 1988; Dougherty, Taylor, & Clark 1991; FTK). Among the sources in our survey, HR 2174A and ζ Lep emit hot dust excesses at relatively short wavelengths ($\sim 8 \mu\text{m}$, as seen in Figs. 14 and 17, respectively). Consequently, HR 2174A and ζ Lep have the largest fractional dust luminosities in our sample, apart from HR 4796A, which is thought to be about 8 ± 2 Myr old (see previous section) and hence might possess a thick disk characteristic of young, pre-main-sequence systems. Sylvester et al. (1996) determined L_{dust}/L_{*} for 22 main-sequence stars and found values ranging from 1.8×10^{-5} to

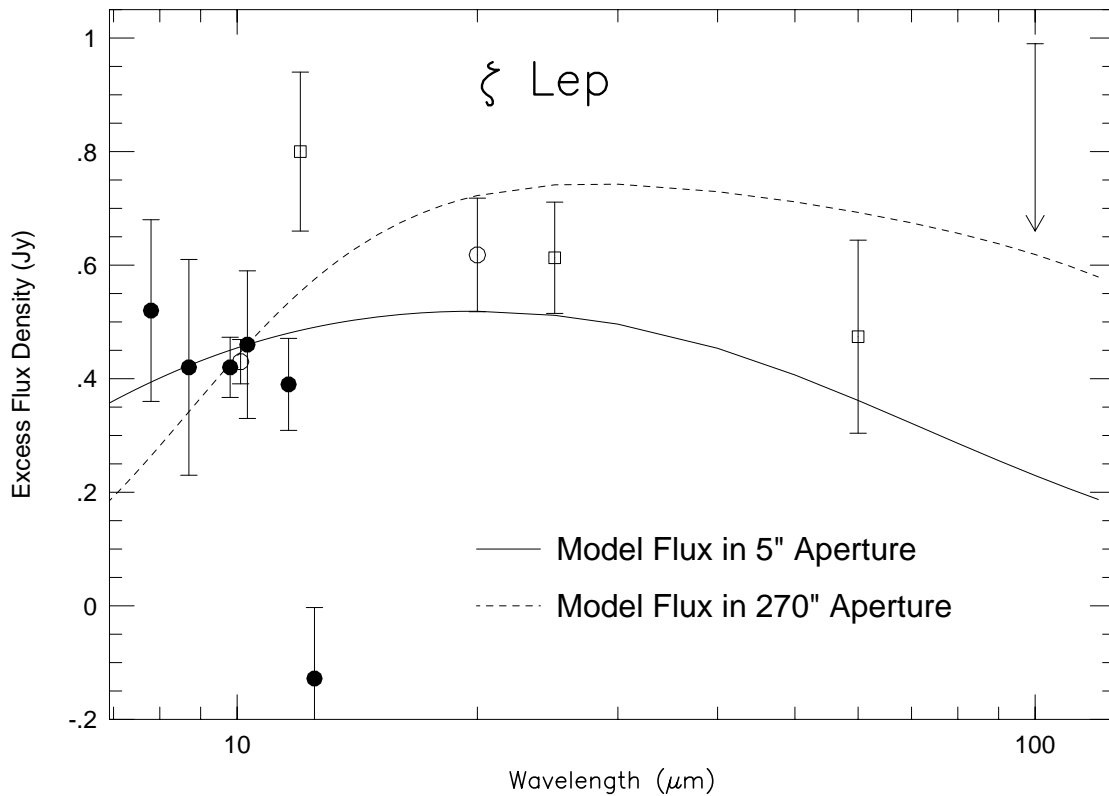


FIG. 17.— ζ Lep excess fluxes after subtraction of the continuum in Fig. 1 or the top panel of Fig. 16; data point symbols are as defined there. Error bars of ground-based data do not include absolute calibration uncertainties. *Solid line*, model flux in a 5" aperture from a shell of blackbody grains extending from 0.5 to 1000 AU from the star, with number density $\propto r^{-1.6}$; *dashed line*, similar model flux in a 270" aperture to mimic that used by Aumann & Probst (1991).

0.64. These authors state that values of $L_{\text{dust}}/L_{\star} > 0.25$ imply additional sources of infrared luminosity, other than thermal reprocessing by dust grains, if these grains are distributed in flat disks around the stars. The grains could instead be distributed in spherical shells, as Sylvester et al. considered, wherein thermal processing alone could account for the above $L_{\text{dust}}/L_{\star}$ values.

4.3. Spatial Extent and Cross-sectional Area of Selected Circumstellar Dust Systems

Section 4.1 described blackbody dust shell models with which we attempted to fit the 10 μm excess emission of the sources listed in Table 6. In these models the shells extend from $r_1 = 0.5\text{--}1$ AU to $r_2 = 2500$ AU (except that $r_2 = 1000$ AU for ζ Lep). These values of r_1 and r_2 are thus very similar among the various models. To further characterize the spatial distribution of dust in the models, we examine the dust density variation with distance from the stars. The exponent γ of radial dependence of volume number density of dust ranges from -0.8 (γ Oph) to -1.8 (β UMa). These exponents γ imply steep radial decreases of grain density around the stars. The quantity of grains in the outer portions of the shells (close to r_2) must therefore be relatively small. As a result, r_2 is uncertain by $\sim 35\%$ in the models.

The above values of γ imply that the location of mid-infrared-emitting dust will be different in the various models. We computed the location of dust in the models that emits most (90%) of the observed mid-infrared (10.3 μm) excess flux. We chose 10.3 μm as the “characteristic” mid-infrared wavelength because it is roughly centered in the 8–12 μm interval spanned by the silicate filters. This spectral

region lets us investigate the conditions of dust at or near solar system terrestrial material temperatures. Table 7 (cols. [2] and [3]) lists inner and outer limits r'_1 and r'_2 (analogous to r_1 and r_2 in Table 6) for the location of blackbody grains emitting 90% of observed excess flux at 10.3 μm . The corresponding dust grain temperatures T'_1 and T'_2 at r'_1 and r'_2 , derived from equation (A1) in the Appendix, are listed in columns (4) and (5).

Table 7 shows that the location and temperature of mid-infrared-emitting dust (cols. [2]–[5]) are very similar in σ Her and γ Oph. In § 4.1, we noted this similarity based on the shape of their model spectra. The mid-infrared-emitting dust is confined within ~ 15 AU from σ Her and γ Oph. In contrast, this dust is much closer to ζ Lep, HR 2174A, and β UMa, within ~ 7 AU from the stars. Table 7 (col. [4]) shows that the highest dust temperatures occur in ζ Lep (960 K) and HR 2174A (800 K) among our sources. In these two systems the grain number density decreases more steeply with distance from the star ($\gamma \sim -1.5$) than in σ Her and γ Oph ($\gamma \sim -0.9$). In β UMa this density decreases even more steeply ($\gamma \sim -1.8$). Therefore, a larger fraction of the mid-infrared-emitting dust grains in ζ Lep, HR 2174A, and β UMa are closer to the star than is the case in σ Her and γ Oph (see below). The latter systems probably have a “hole” in their circumstellar dust distributions, as previously inferred from their excess spectral shapes (§ 4.1).

In Table 7 (cols. [6] and [7]), we list the median radial distance from the star $r'_{1/2}$, and corresponding temperature $T'_{1/2}$, of the grains in the shell within r'_1 and r'_2 (cols. [2] and [3]). The Appendix describes the computation of $r'_{1/2}$ and $T'_{1/2}$. These quantities can be regarded as the characteristic

TABLE 7
MODELS OF 90% OF 10.3 μm EXCESS

Name (1)	r'_1 (AU) (2)	r'_2 (AU) (3)	T'_1 ^a (K) (4)	T'_2 ^a (K) (5)	$r'_{1/2}$ ^b (AU) (6)	$T'_{1/2}$ ^c (K) (7)	Area ^d (cm^2) (8)
σ Her	1	16	790	200	11.5	238	8×10^{24}
γ Oph	1	15	740	200	11	227	2×10^{24}
HR 2174A	0.5	6	800	240	3.9	292	8×10^{24}
β UMa	1	7	690	260	4.2	337	4×10^{23}
ζ Lep	0.5	7	960	250	4.3	317	2×10^{24}

NOTES.—Models are as described in Table 6; $r'_1 = r_1$, and r'_2 is smaller than r_2 to include only the hottest dust grains. Models produce 90% of the observed flux at 10.3 μm .

^a T'_1 and T'_2 are radiative equilibrium temperatures at the inner and outer shell boundaries r'_1 and r'_2 , respectively. These temperatures are obtained via eq. (A1) in the Appendix.

^b Median grain radial distance r from the star.

^c Median grain radiative equilibrium temperature.

^d Geometric cross-sectional area of all dust grains that would be observed in a 5" beam.

location and temperature of mid-infrared-emitting blackbody grains around the stars. In systems with steep radial density decrease (ζ Lep, HR 2174A, and β UMa), $r'_{1/2}$ is smaller (~ 4 AU) than in systems with a flatter density decrease (σ Her and γ Oph), where $r'_{1/2} \sim 11$ AU. It can be seen from Table 7 (col. [7]) that the median dust temperatures of ζ Lep, HR 2174A, and β UMa are ~ 300 K or above. In σ Her and γ Oph these temperatures are below ~ 240 K. These model results give us insights on the locations where dust at temperatures close to those of Earth-like planets will interfere with future searches for such planets (Backman 1998).

The mass of blackbody grains around these stars is difficult to determine because of the unknown grain sizes. However, we can quantify the amount of dust unambiguously by computing the total cross-sectional area of grains. This quantity is independent of grain size if we assume all grains to emit as blackbodies. Equation (A4) summarizes the pertinent calculations. The last column of Table 6 lists the cross-sectional area of all blackbody dust grains contained in the 5" observation beam, for each of our sources.

The range of grain areas of the systems in Table 6 is comparable to that of α Lyr, α PsA, β Pic, and ϵ Eri (6×10^{26} to 8×10^{29} cm^2 ; Gillett 1986). The latter were computed across the entire dust distributions (disks) bounded by their inner and outer radii. These dust distributions would fit entirely within the *IRAS* beam. We computed the grain area of only those portions of the dust distribution within our observation beam. Our computed grain areas would thus be smaller than in Gillett's (1986) models. However, the quantity of excluded outermost dust grains is small because of the steep radial gradients implied by γ .

We also computed the cross-sectional area of blackbody grains responsible for 90% of the 10.3 μm excess emission (i.e., grains within the radial limits r'_1 and r'_2 in Table 7, cols. [2] and [3]). The resulting grain areas are listed in Table 7, column (8). For comparison, the cross-sectional area of dust grains around β Pic within 30 AU from the star, in a disk model by Knacke et al. (1993), is $\sim 6 \times 10^{25}$ cm^2 . This grain area is larger than those of mid-infrared-emitting grains in the systems in Table 7. The 10 μm excess of β Pic is more prominent than that of any of our sources. The β Pic excess

is 1.2 Jy, or 44% of the total 10 μm flux density. The quantity of mid-infrared-emitting dust around β Pic is evidently larger than in the systems we observed. As another comparison, the cross-sectional area of 10 μm -emitting dust around 51 Oph is $\sim 2 \times 10^{26}$ cm^2 , as inferred from the mass estimate by FTK. In this estimate, all grains were assumed to be 5 μm in radius and at 500 K. This temperature is higher than the median temperatures $T'_{1/2}$ (Table 7, col. [7]) of our sources. Otherwise, the assumptions in the grain area estimate around 51 Oph are very similar to those made in this section. The grain cross-sectional area around 51 Oph is larger than those of β Pic and any of our sources in Table 7. This grain area would be even larger if FTK had assumed blackbody grains (instead of 5 μm ones). It is possible that, as in the case of β Pic and 51 Oph, small and optically thin dust grains also emit the observed excesses of our sources. Their emissivities will be determined when higher S/N fluxes become available, such as from photometry and spectroscopy with *ISO*. In that case one will be able to directly compare the quantity of optically thin dust grains around these sources and 51 Oph and β Pic.

5. CONCLUSIONS

We have obtained mid-infrared small-aperture (4"–5" diameter beam) photometry for 10 Vega-type stars. Five of these sources (68 Oph, HR 10, 21 LMi, α PsA, and HR 4796A) do not show any excess at ~ 10 μm . We did not detect prominent emission in the silicate feature from any of the sources we observed. σ Her and γ Oph exhibit excess flux increasing with wavelength, for wavelengths greater than 10 μm . The only source whose excess flux (at *IRAS* wavelengths) could be fitted by a single-temperature blackbody was HR 4796A. The rest of the sources' excess spectra can be crudely fitted by multitemperature dust distributions. ζ Lep and HR 2174 show evidence for excess flux at short wavelengths (~ 8 μm), implying hot dust grains located close to the stars. We found marginal evidence for the possibility of weak silicate emission in the excess spectra of ζ Lep and β UMa. We found significant amounts of dust at or near solar system terrestrial material temperatures around HR 2174A, ζ Lep, and β UMa.

Our data for the 10 sources constitute the most accurate determination to date of the excess emission from the immediate vicinity of the stars. The simple models that we fitted

to these data give us an idea of the temperatures and radial density distribution of dust grains. In these models we assumed all dust grains to be blackbodies. This assumption is plausible because of the absence of prominent emission features in our data. β UMa could be an exception if its 11 μm excess is confirmed to be from silicate emission. The S/N of our data is not sufficiently high to unambiguously identify emission from a silicate feature. This identification will be possible with photometry and spectroscopy from *ISO*. Future ground-based and space observations will also reveal the geometry of the circumstellar dust regions. These data will yield unambiguous density profiles and masses of shells or disks. This characterization of circumstellar structure will be a valuable input in assessing the conditions under which stars and planetary systems form and evolve,

and what the prospects are for detections of mature planetary systems.

We thank Keith Noll for assistance with IRTF observations, Robert Kurucz for providing the model atmospheres to SUNY Stony Brook, and the anonymous referee for constructive comments. The work has made use of the SIMBAD database, operated at CDS, Strasbourg, France. This research was supported at the University of Denver by grants NAGW-3680 and NAG 5-3411 from the NASA *ISO* Key Project program, at Penn State Erie by grant NAGW-3415 from the NASA Planetary Astronomy Program, Office of Space Science, and at SUNY Stony Brook by grant NAGW-2334 from the NASA Origins of Solar Systems research program.

APPENDIX

THERMAL MODELS OF BLACKBODY GRAINS

The modeling of infrared excess flux densities followed the general procedures of Backman et al. (1992) and Knacke et al. (1993). We assumed the dust to be distributed in a spherical shell around each of our sources. A unit volume in the shell, located at a distance r from the star, contains $n(r_0)(r/r_0)^\gamma$ grains, where r_0 is a reference distance. Grains in these models are assumed to be blackbodies, but their sizes (radii) a are not constrained by our observations and models. Their absorptive and emissive efficiencies are unity, and their geometric albedo is zero. Their radiative equilibrium temperatures at r are

$$T(r) = 278[R_*/(1 R_\odot)]^{1/2}[T_*/(1 T_\odot)]r^{-1/2} \quad (\text{A1})$$

[$R_*/(1 R_\odot)$ and $T_*/(1 T_\odot)$ being the radius and temperature of the stellar source in solar units].

The flux density at Earth from particles between r and $r + dr$, inside the observation beam, is

$$f(r) = \frac{G(r)}{D^2} n(r_0) \left(\frac{r}{r_0}\right)^\gamma \pi a^2 B[T(r), \lambda] dr \quad (\text{Jy}), \quad (\text{A2})$$

where $B[T(r), \lambda]$ is the Planck function in Jy sr^{-1} , D is the distance from the observer to the star, and $G(r)$ is a factor dependent on the geometry of the dust region. In the case of spherical shell configurations, $G(r) = 4\pi r^2$.

We did not model disk configurations, but in § 4.1 we compared them with shell configurations. Two types of disks that we considered are flaring disks with thickness $z(r)$ proportional to r [$z(r) = z_0 r$], and flat disks [$z(r) = z_0$]. In these two cases, $G(r) = 2\pi r z(r)$. Apart from a normalization constant (dependent on z_0), equation (A2) shows that the model flux density $f(r)$ from a flaring disk is similar to that from a shell, if both have the same γ . The model flux density from a flat disk is also similar to that from the above shell, if the disk density exponent is $\gamma + 1$ (eq. [A2]).

The flux density at Earth from all dust grains within $r_1 \leq r \leq r_2$ from the star, and inside the observation beam, is

$$F = \int_{r_1}^{r_{\text{beam}}} f(r) dr + \int_{r_{\text{beam}}}^{r_2} \eta(r) f(r) dr \quad (\text{Jy}), \quad (\text{A3})$$

where r_{beam} is the radius subtended by the observation beam at the source position and $\eta(r)$ is the fraction of dust grains within r and $r + dr$, for $r > r_{\text{beam}}$, that are inside the observation beam. For spherical shells, $\eta(r) \approx \frac{1}{2} \arcsin^2(r_{\text{beam}}/r)$ while, for disks, $\eta(r) \approx (2/\pi) \arcsin(r_{\text{beam}}/r)$, if $D \gg r$. The choice of disk or shell models will affect the flux computations [through $\eta(r)$] only at $r > r_{\text{beam}}$, where dust does not contribute significantly to mid-infrared model flux densities.

The cross-sectional area of dust grains in a spherical shell, and within the observation beam, is

$$C = 4\pi^2 r_0^2 n(r_0) a^2 \left[\int_{r_1}^{r_{\text{beam}}} (r/r_0)^{\gamma+2} dr + \int_{r_{\text{beam}}}^{r_2} (r/r_0)^{\gamma+2} \eta(r) dr \right] \quad (\text{cm}^2). \quad (\text{A4})$$

The cross-sectional area C is independent of blackbody grain size a for a given shell model and flux density F . The reason is that the product $n(r_0)a^2$ above is determined by the normalization of model to observed flux density in equations (A2) and (A3).

Let $r_{1/2}$ be the median radial distance of grains from the star. To obtain $r_{1/2}$, we found, via equation (A4), the radial distance $r_{1/2}$ at which the grain cross-sectional area contained within r_1 and $r_{1/2}$ is half that within r_1 and r_2 . The number of grains within r_1 and $r_{1/2}$ is also one-half the number between r_1 and r_2 , because the grain size is assumed constant across the shell. The median temperature $T_{1/2}$ is found by substituting $r_{1/2}$ in equation (A1).

REFERENCES

- Aitken, D. K., Moore, T. J. T., Roche, P. F., Smith, C. H., & Wright, C. M. 1993, *MNRAS*, 265, L41
- Allen, D. A. 1973, *MNRAS*, 161, 145
- Aumann, H. H. 1985, *PASP*, 97, 885
- Aumann, H. H., et al. 1984, *ApJ*, 278, L23
- Aumann, H. H., & Probst, R. G. 1991, *ApJ*, 368, 264
- Backman, D. E. 1998, in *Proc. Exozodiacal Dust Working Conference*, ed. D. E. Backman et al. (Washington, DC: GPO), in press
- Backman, D., & Gillett, F. C. 1987, in *Cool Stars, Stellar Systems, and the Sun*, ed. J. L. Linsky & R. E. Stencel (Berlin: Springer), 340
- Backman, D. E., Gillett, F. C., & Witteborn, F. C. 1992, *ApJ*, 385, 680
- Backman, D. E., & Paresce, F. 1993, in *Protostars and Planets III*, ed. E. H. Levy, J. I. Lunine, & M. S. Mathews (Tucson: Univ. Arizona Press), 1253
- Bessell, M. S., & Brett, J. M. 1988, *PASP*, 100, 1134
- Blackwell, D. E., Booth, A. J., Petford, A. D., Leggett, S. K., Mountain, C. M., & Selby, M. J. 1986, *MNRAS*, 221, 427
- Bless, R. C., & Savage, B. D. 1982, *ApJ*, 171, 293
- Campins, H., & Ryan, E. 1989, *ApJ*, 341, 1059
- Cheng, K.-P., Grady, C. A., & Bruhweiler, F. C. 1991, *ApJ*, 366, L87
- Code, A. D., Davis, J., Bless, R. C., & Hanbury Brown, R. 1976, *ApJ*, 203, 417
- Cohen, M., Walker, R. G., Barlow, M. J., & Deacon, J. R. 1992, *AJ*, 104, 1650
- Coulson, I. M., & Walther, D. M. 1995, *MNRAS*, 274, 977
- Dougherty, S. M., Taylor, A. R., & Clark, T. A. 1991, *AJ*, 102, 1753
- Draine, B. T., & Lee, H. M. 1984, *ApJ*, 285, 89
- Fajardo-Acosta, S. B. 1996, in *IAU Colloq. 150, Physics, Chemistry, and Dynamics of Interplanetary Dust*, ed. B. A. S. Guftason & M. S. Hanner (ASP Conf. Ser. 104) (Provo: ASP Press), 507
- Fajardo-Acosta, S. B., Telesco, C. M., & Knacke, R. F. 1993, *ApJ*, 417, L33 (FTK)
- FitzGerald, M. P. 1970, *A&A*, 4, 234
- Gillett, F. C. 1986, in *Light on Dark Matter*, ed. F. P. Israel (Dordrecht: Reidel), 61
- Grady, C. A., Bruhweiler, F. C., Cheng, K.-P., & Chiu, W. A. 1991, *ApJ*, 367, 296
- Habing, H. J., et al. 1996, *A&A*, 315, L233
- Hanner, M. S., Lynch, D. K., & Russell, R. W. 1994, *ApJ*, 425, 274
- Hanner, M. S., & Tokunaga, A. T. 1991, in *Comets in the Post-Halley Era*, Vol. 1, ed. R. L. Newburn et al. (Dordrecht: Kluwer), 67
- Hoffleit, D., & Jaschek, C. 1982, *The Bright Star Catalogue* (New Haven: Yale Univ. Obs.)
- IRAS Catalogs and Atlases: Explanatory Supplement*. 1988, ed. C. A. Beichman, G. Neugebauer, H. J. Habing, P. E. Clegg, & T. J. Chester (Washington: GPO) (ES)
- IRAS Point Source Catalog, Version 2*. 1988, Joint *IRAS Science Working Group* (Washington: GPO) (PSC)
- IRTF Observer's Manual*. 1986, NASA Infrared Telescope Facility (Honolulu: Univ. Hawaii)
- Jenkins, L. F. 1963, *General Catalogue of Trigonometric Stellar Parallaxes* (New Haven: Yale Univ. Obs.)
- Johnson, H. L. 1965, *Commun. Lunar Planet. Lab.*, 3, 73
- . 1966, *ARA&A*, 4, 193
- Johnson, H. L., Iriarte, B., Mitchell, R. I., & Wisniewski, W. Z. 1966, *Commun. Lunar Planet. Lab.*, 4, 99
- Jura, M. 1991, *ApJ*, 383, L79
- Jura, M., Ghez, A. M., White, R. J., McCarthy, D. W., Smith, R. C., & Martin, P. G. 1995, *ApJ*, 445, 451
- Jura, M., Zuckerman, B., Becklin, E. E., & Smith, R. C. 1993, *ApJ*, 418, L37
- Knacke, R. F., Fajardo-Acosta, S. B., Telesco, C. M., Hackwell, J. A., Lynch, D. K., & Russell, R. W. 1993, *ApJ*, 418, 440
- Koorneef, J. 1983, *A&AS*, 51, 489
- Kurucz, R. L. 1979, *ApJS*, 40, 1
- . 1991, in *Precision Photometry: Astrophysics of the Galaxy*, ed. A. G. D. Philip, A. R. Uggren, & K. A. Janes (Schenectady: L. Davis), 27
- . 1992, in *IAU Symp. 149, Stellar Populations of Galaxies*, ed. B. Barbuy & A. Renzini (Dordrecht: Kluwer), 225
- Lagrange-Henri, A. M., Ferlet, R., Vidal-Madjar, A., Beust, H., Gry, C., & Lallement, R. 1990, *A&AS*, 85, 1089
- Lagrange-Henri, A. M., Vidal-Madjar, A., & Ferlet, R. 1988, *A&A*, 190, 275
- Leggett, S. K., Bartholomew, M., Mountain, C. M., & Selby, M. J. 1986, *MNRAS*, 223, 443
- Malagini, M. L., & Morossi, C. 1990, *A&AS*, 85, 1015
- Merrill, K. M. 1974, *Icarus*, 23, 566
- Nandy, K., Thompson, G. I., Jamar, C., Monfils, A., & Wilson, R. 1976, *A&A*, 51, 63
- Oudmaijer, R. D., van der Veen, W. E. C. J., Waters, L. B. F. M., Trams, N. R., Waelkens, C., & Engelsman, E. 1992, *A&AS*, 96, 625
- Russell, R. W., Lynch, D. K., Hackwell, J. A., Fajardo-Acosta, S. B., Knacke, R. F., Hanner, M. S., & Telesco, C. M. 1998, in preparation
- Sadakane, K., & Nishida, M. 1986, *PASP*, 98, 685
- Savage, B. D., & Mathis, J. S. 1979, *ARA&A*, 17, 73
- Skinner, C. J., Barlow, M. J., & Justtanont, K. 1992, *MNRAS*, 255, 31P
- Skinner, C. J., Sylvester, R. J., Graham, J. R., Barlow, M. J., Meixner, M., Keto, E., Arens, J. F., & Jernigan, J. G. 1995, *ApJ*, 444, 861
- Smalley, D., & Dworetzky, M. M. 1995, *A&A*, 293, 446
- Stauffer, J. R., Hartmann, L. W., & Barrado y Navascues, D. 1995, *ApJ*, 454, 910
- Sylvester, R. J., Skinner, C. J., Barlow, M. J., & Mannings, V. 1996, *MNRAS*, 279, 915
- Telesco, C. M., & Knacke, R. F. 1991, *ApJ*, 372, L29 (TK)
- Telesco, C. M., Becklin, E. E., Wolstencroft, R. D., & Decher, R. 1988, *Nature*, 335, 51
- Thompson, G. I., Nandy, K., Jamar, C., Monfils, A., Houziaux, L., Carnochan, D. J., & Wilson, R. 1978, *Catalog of Stellar Ultraviolet Fluxes* (ESA SR-28)
- Tokunaga, A. T. 1984, *AJ*, 89, 172
- . 1986, *NASA IRTF Photometry Manual* (Honolulu: Univ. Hawaii)
- Vidal-Madjar, A., Ferlet, R., Lecavelier des Etangs, A., Perrin, G., & Sèvre, F. 1993, *IAU Circ.* 5795
- Vidal-Madjar, A., et al. 1995, *Ap&SS*, 223, 198
- Waelkens, C., et al. 1996, *A&A*, 315, L245
- Walker, H. J., & Butner, H. M. 1995, *Ap&SS*, 224, 389
- Walker, H. J., & Wolstencroft, R. D. 1988, *PASP*, 100, 1059
- Waters, L. B. F. M., Coté, J., & Aumann, H. H. 1987, *A&A*, 172, 225
- Waters, L. B. F. M., Coté, J., & Geballe, T. R. 1988, *A&A*, 203, 348
- Waters, L. B. F. M., et al. 1995, *A&A*, 299, 173
- Wesselius, P. R., de Jonge, A. R. W., Kester, D. J. M., & Roelfsema, P. R. 1992, in *Infrared Astronomy with ISO*, ed. T. Encrenaz & M. F. Kessler (Commack: Nova Sci.), 509
- Witteborn, F. C., Bregman, J. D., Lester, D. F., & Rank, D. M. 1982, *Icarus*, 50, 63
- Zuckerman, B., & Becklin, E. E. 1993, *ApJ*, 406, L25